

## A SPECTROSCOPIC SURVEY OF REDSHIFT $1.4 \lesssim z \lesssim 3.0$ GALAXIES IN THE GOODS-NORTH FIELD: SURVEY DESCRIPTION, CATALOGS, AND PROPERTIES<sup>1</sup>

NAVEEN A. REDDY<sup>2,3</sup>, CHARLES C. STEIDEL<sup>2</sup>, DAWN K. ERB<sup>4</sup>, ALICE E. SHAPLEY<sup>5</sup>, AND MAX PETTINI<sup>6</sup>

*Received 2006 June 23; Accepted 2006 September 01*

### ABSTRACT

We present the results of a spectroscopic survey with the Low Resolution Imaging Spectrograph on the Keck I telescope of more than 280 star-forming galaxies and AGN at redshifts  $1.4 \lesssim z \lesssim 3.0$  in the GOODS-North field. Candidates are selected by their  $U_nGR$  colors using the “BM” and “BX” criteria to target redshift  $1.4 \lesssim z \lesssim 2.5$  galaxies and the Lyman break criteria to target redshift  $z \sim 3$  galaxies; combined these samples account for  $\sim 25 - 30\%$  of the R and  $K_s$ -band counts to  $\mathcal{R} = 25.5$  and  $K_s(\text{AB}) = 24.4$ , respectively. The sample of 212 BM/BX galaxies and 74 LBGs is presently the largest spectroscopic sample of galaxies at  $z > 1.4$  in GOODS-N, and includes 19 spectroscopically-confirmed distant red galaxies (DRGs) with  $J - K_s > 2.3$  (Vega). Extensive multi-wavelength data, including our very deep ground-based near-IR imaging to  $K_s(\text{AB}) = 24.4$ , allow us to investigate the stellar populations, stellar masses, bolometric luminosities ( $L_{\text{bol}}$ ), and extinction of  $z \sim 2$  galaxies. Deep *Chandra* X-ray and *Spitzer* IRAC and MIPS data indicate that the sample includes galaxies with a wide range in  $L_{\text{bol}}$ , from  $\simeq 10^{10} L_{\odot}$  to  $> 10^{12} L_{\odot}$ , and covering 4 orders of magnitude in dust obscuration ( $L_{\text{bol}}/L_{\text{UV}}$ ). The sample includes galaxies with a large dynamic range in evolutionary state, from very young galaxies (ages  $\simeq 50$  Myr) with small stellar masses ( $M^* \simeq 10^9 M_{\odot}$ ) to evolved galaxies (ages  $> 2$  Gyr) with stellar masses comparable to the most massive galaxies at these redshifts ( $M^* > 10^{11} M_{\odot}$ ). *Spitzer* data indicate that the optical sample includes some fraction of the obscured AGN population at high redshifts: at least 3 of 11 AGN in the  $z > 1.4$  sample are undetected in the deep X-ray data but exhibit power-law SEDs longward of  $\sim 2 \mu\text{m}$  (rest-frame) indicative of obscured AGN. The results of our survey indicate that rest-frame UV selection and spectroscopy presently constitute the most time-wise *efficient* method of culling large samples of high redshift galaxies with a wide range in intrinsic properties, and the data presented here will add significantly to the multi-wavelength legacy of the GOODS survey.

*Subject headings:* cosmology: observations — galaxies: active — galaxies: evolution — galaxies: high redshift — galaxies: starburst — galaxies: stellar content

### 1. INTRODUCTION

Rapid advances in our understanding of galaxy evolution have been prompted by the recognition that observations covering the full spectrum are necessary to adequately interpret the physical nature of galaxies. Multi-color *Hubble Space Telescope* (*HST*) imaging of two otherwise inconspicuous fields in the high Galactic latitude sky (Williams et al. 1996, 2000) marked the inception of a decade dominated by large-scale multi-wavelength surveys. The two *Hubble* Deep Fields are now encompassed or supplanted by other areas of the sky which are the focus of a number of space and ground-based observations both within and peripheral to the *Great Observatories Origins Deep Survey* (GOODS; Dickinson et al. 2003a). Included among these data are the deepest *Chandra* X-

ray observations (Alexander et al. 2003), *HST* ACS optical imaging (Giavalisco et al. 2004), *Spitzer* IR to far-IR imaging (Dickinson et al., in prep; Chary et al., in prep), *GALEX* far and near-UV imaging (Schiminovich et al. 2003), ground-based optical and near-IR imaging and spectroscopy (Capak et al. 2004; Cowie et al. 2004; Vanzella et al. 2005), and radio/submillimeter observations (Richards 2000; Pope et al. 2005).

Despite the easy access to broadband photometry and subsequent insights into galaxy evolution made possible by multi-wavelength surveys such as GOODS, important issues regarding survey completeness and the physical conditions in galaxies and their surrounding intergalactic medium can only be investigated spectroscopically. Spectroscopy of galaxies in blind flux-limited surveys can be quite inefficient and expensive, particularly if one only wants to study galaxies at certain cosmological epochs. However, we have shown that the technique of photometric pre-selection can allow one to cull large samples of galaxies in particular redshift ranges over a large range in redshift  $1.0 \lesssim z \lesssim 4$  (e.g., Adelberger et al. 2004; Steidel et al. 2004, 2003, 1995; Steidel & Hamilton 1993), which can then be efficiently followed up using multi-object optical spectrographs such as the Low Resolution Imaging Spectrograph (LRIS) on the 10 m Keck telescope. Near-UV sensitive spectrographs such as the blue arm of LRIS (LRIS-B) on Keck and the Focal Reducer/low dispersion Spectro-

<sup>1</sup> Based on data obtained at the W.M. Keck Observatory, which is operated as a scientific partnership among the California Institute of Technology, the University of California, and NASA, and was made possible by the generous financial support of the W.M. Keck Foundation.

<sup>2</sup> California Institute of Technology, MS 105-24, Pasadena, CA 91125

<sup>3</sup> NOAO, 950 N Cherry Ave, Tucson, AZ 85719

<sup>4</sup> Harvard-Smithsonian Center for Astrophysics, 60 Garden Street, Cambridge, MA 02138

<sup>5</sup> Department of Astrophysical Sciences, Peyton Hall-Ivy Lane, Princeton, NJ 08544

<sup>6</sup> Institute of Astronomy, Madingley Road, Cambridge CB3 OHA, UK

graph (FORS) on the VLT have significantly extended our capabilities by allowing for spectroscopy of key features that fall shortward of the OH emission forest for redshifts  $1.4 \lesssim z \lesssim 3$ , a particularly active epoch in the context of galaxy evolution and the buildup of stellar and black hole mass. To take advantage of extensive multi-wavelength data, we included the GOODS-North (GOODS-N, hereafter) field in our ongoing survey to select and spectroscopically followup large samples of galaxies at redshifts  $1.4 \lesssim z \lesssim 3.0$  (Steidel et al. 2004). In the interest of public dissemination of data, we present in this paper the results of our spectroscopic survey of  $1.4 \lesssim z \lesssim 3.0$  star-forming galaxies in the GOODS-N field including associated photometry and spectroscopic redshifts. Information on the galaxies, including their photometric measurements and errors and stellar population fits, are available at the following public website: <http://www.astro.caltech.edu/~drlaw/GOODS/>.

The outline of this paper is as follows. In § 2 we briefly describe the optical imaging, photometry, and spectroscopy. To supplement these, we have also obtained the deepest wide-area near-IR  $J$  and  $K_s$ -band imaging in the GOODS-North field, and these data are also presented in § 2. The spectroscopic results and associated catalog are presented in § 3. We describe the *Spitzer* IRAC and MIPS data (taken from the GOODS-N public release; Dickinson et al. in prep. and Chary et al. in prep.) for our spectroscopic sample of galaxies in § 4. Ground-based photometry and *Spitzer* IRAC data, together with spectroscopic redshifts, enable the modeling of the stellar populations of galaxies given certain simplifying assumptions. Our modeling procedure and results are discussed in § 5. In § 6 we describe a few characteristics of the sample of star-forming galaxies and AGN to demonstrate the wide range in intrinsic properties of UV-selected galaxies at high redshift. A flat  $\Lambda$ CDM cosmology is assumed with  $H_0 = 70 \text{ km s}^{-1} \text{ Mpc}^{-1}$  and  $\Omega_\Lambda = 0.7$ . All magnitudes are on the AB (Oke & Gunn 1983) system.

## 2. DATA AND SAMPLE SELECTION

### 2.1. Optical and Near-IR Imaging and Photometry

The imaging, photometry, color selection, and spectroscopic observations of galaxies in the fields of our  $z \sim 2$  survey are described in several other papers published by our group (Steidel et al. 2003, 2004; Adelberger et al. 2004; Reddy et al. 2005). Specific details regarding the GOODS-N optical imaging are presented in Reddy et al. (2005) and summarized below for convenience.

The optical images used to photometrically pre-select candidate galaxies at redshifts  $1.4 \lesssim z \lesssim 3.0$  in the GOODS-N field were obtained in 2002 and 2003 April with the KPNO and Keck I telescopes. The KPNO MOSAIC  $U$ -band image obtained from the GOODS team (PI: Giavalisco) was transformed to  $U_n$  magnitudes (Steidel et al. 2004). The Keck I  $G$ - and  $R$ -band images were taken with the LRIS instrument (Oke et al. 1995; Steidel et al. 2004) and were oriented to ensure maximum overlap with the GOODS *Spitzer* Legacy and *Hubble* Treasury programs. The images cover  $11' \times 15'$  with  $\text{FWHM} \sim 0''.7 - 1''.1$  to a limiting magnitude of  $\sim 27.5$  measured within a  $1''$  aperture ( $3\sigma$ ) in the  $U_nGR$  bands. This depth ensures we are complete to  $\mathcal{R} = 25.5$ , neglecting photometric scatter, for galaxies whose colors

satisfy our  $z \sim 2 - 3$  color criteria. The optical imaging reduction and photometry were done following the procedures described in Steidel et al. (2003, 2004). The images were astrometrically calibrated using the SDSS database. Source detection is done at  $\mathcal{R}$ -band, and  $G - \mathcal{R}$  and  $U_n - G$  colors are computed by applying the  $\mathcal{R}$ -band isophotal apertures to images in the other filters.

We have obtained very deep wide-area near-IR imaging at  $J$  and  $K_s$ -band in the GOODS-N field from observations with the Wide Field Infrared Camera (WIRC; Wilson et al. 2003) on the Palomar Hale 5 m telescope. The images, taken under photometric conditions with  $\sim 1''.0$  FWHM, reach a depth of  $K_s \sim 24.4$  and  $J \sim 25.0$  over the central  $8''.7 \times 8''.7$  of the GOODS-N field. The near-IR imaging reduction procedure is described in detail by Erb et al. (2006c). Near-IR magnitudes were calibrated in Vega magnitudes and converted to AB units assuming the following conversions:  $K_s(AB) = K_s(\text{Vega}) + 1.82$  and  $J(AB) = J(\text{Vega}) + 0.90$ . Figure 1 shows the area imaged in the near-IR with respect to our optical image of the GOODS-N field.

Photometric errors for both optical and near-IR magnitudes were determined from Monte Carlo simulations. We added large numbers of simulated galaxies with known magnitudes to our images and then recovered them using the same photometric method used to detect actual galaxies. Comparing the input magnitudes with those recovered then yields an estimate of the bias and uncertainty in our photometry. The Monte Carlo method is discussed in more detail by Shapley et al. (2005). The typical errors in the optical and near-IR magnitudes range from 0.05 to 0.3 mag.

### 2.2. Photometric Selection

We selected galaxies in different redshift ranges between  $1.4 \lesssim z \lesssim 3.4$  using the “BM”, “BX”, “C”, “D”, and “MD” selection criteria (Steidel et al. 2003; Adelberger et al. 2004; Steidel et al. 2004). The “C”, “D”, and “MD” criteria are used to select Lyman Break Galaxies (LBGs) at redshifts  $2.7 \lesssim z \lesssim 3.3$  (Steidel et al. 2003)<sup>7</sup>. The “BM” and “BX” criteria were designed to cull galaxies at redshifts  $1.4 \lesssim z \lesssim 2.0$  and  $2.0 \lesssim z \lesssim 2.5$ , respectively, with approximately the same range of UV luminosity and intrinsic UV color as the  $z \sim 3$  LBGs (Adelberger et al. 2004; Steidel et al. 2004). The various selection criteria considered here are shown in Figure 2. We only considered candidates to  $\mathcal{R} = 25.5$  to ensure a sample of galaxies which are bright enough such that optical spectroscopy is feasible<sup>8</sup>. This limit corresponds to an absolute magnitude 0.6 mag fainter at  $z \sim 2.2$  than at  $z \sim 3$ , based on the distance modulus between the two redshifts. We also excluded from the sample those candidates with  $\mathcal{R} < 19$  since almost all of these objects are stars. Optical selection yielded 1360 BM/BX and 192 C/D/MD candidates in the  $11' \times 15'$  area of the

<sup>7</sup> Note that we did not select “M” galaxies in GOODS-N as was done in other fields of the  $z \sim 3$  survey (Steidel et al. 2003).

<sup>8</sup> A few objects were candidates based on photometry of our *Palomar* images of the GOODS-N field (Steidel et al. 2003), but failed to satisfy the photometric selection criteria based on the newer *Keck* images. These objects are indicated in subsequent tables by their notation as presented in Steidel et al. (2003) or, in the case of BM/BX objects, by the letters “BX” or “BM” followed by no more than 3 numerical digits. The photometric values for these objects are the ones based on the new photometry.

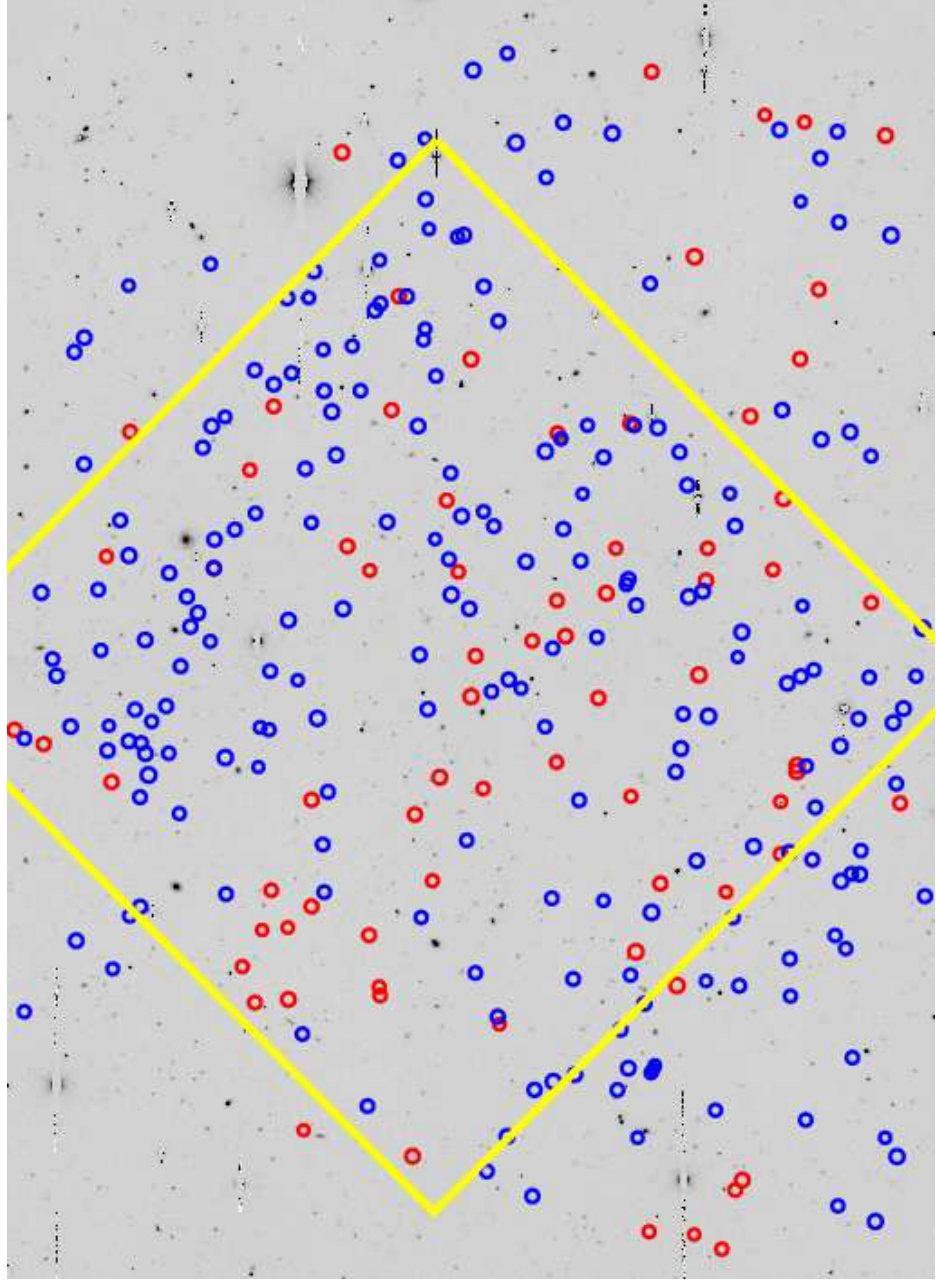


FIG. 1.— Positions of BX/BM (blue circles) and LBG (red circles) galaxies with spectroscopic redshifts  $z > 1.4$  overlaid on our  $10' \times 15'$  optical  $\mathcal{R}$ -band image of the GOODS-N field. The yellow box ( $8.5' \times 8.5'$ ) indicates the region with deep  $J$  and  $K_s$  Palomar imaging.

GOODS-N field. Combined, the BX/BM and C/D/MD candidates constitute  $\sim 30\%$  of the  $\mathcal{R}$ -band counts to  $R = 25.5$ . The number of candidates and their surface densities are listed in Table 1. Approximately 50% of these candidates lie in the region imaged at  $J$  and  $K_s$ . The remainder of this paper focuses on those galaxies which have been spectroscopically confirmed to lie at redshifts  $z > 1.4$ , as described in the next section.

### 2.3. Optical Spectroscopy

We took advantage of the multi-object capabilities of the Keck LRIS instrument to obtain spectroscopy for the photometrically selected candidates. In its upgraded double-armed capacity, LRIS makes use of a dichroic to send light to both a red and blue arm. The commissioning of the blue arm of LRIS (LRIS-B) allowed, for

the first time, the ability to obtain very sensitive near-UV spectroscopic observations at wavelengths as short as  $\sim 3100 \text{ \AA}$ , essentially to the atmospheric transmission limit. The wavelength range from the atmospheric cutoff up to  $\sim 5500 \text{ \AA}$  is particularly useful for probing the rich set of interstellar and stellar lines between Ly $\alpha$  and C IV ( $\lambda 1548, 1550$ ) for galaxies in the so-called “spectroscopic desert”, between redshifts  $1.4 \lesssim z \lesssim 2.5$ . As shown previously in Adelberger et al. (2004) and Steidel et al. (2004), combining photometric selection of BM and BX candidates with the near-UV sensitivity of LRIS-B allows for the wholesale spectroscopy of large numbers of galaxies in this redshift range; this in turn enables us to focus our study on an epoch that was particularly active in terms of star formation and accretion activity (e.g., Dickinson et al. 2003b; Chapman et al. 2003;

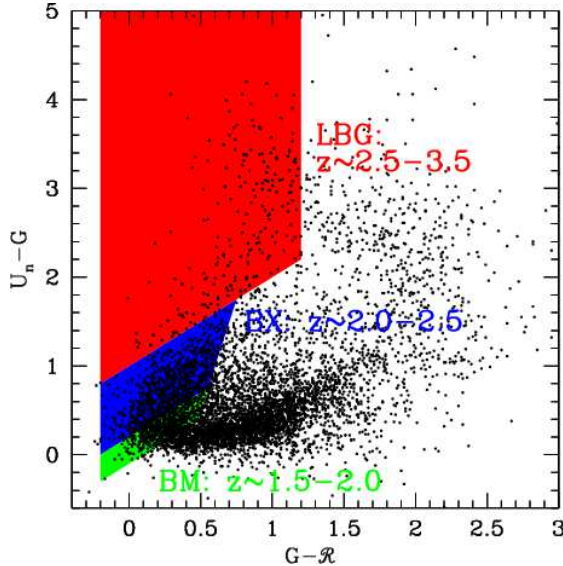


FIG. 2.—  $U_nGR$  colors of objects with  $\mathcal{R} < 25.5$  in the GOODS-N field. Also shown are the LBG, BX, and BM selection windows.

Fan et al. 2001; Madau et al. 1996; Shaver et al. 1996; Schmidt et al. 1995).

The instrumental setup used for spectroscopy in the GOODS-N field varied during the course of the  $z \sim 2$  survey; the various setups are described in more detail by Steidel et al. (2004). We selected dichroic filters designed to split the incoming beam at 5600 Å or 6800 Å. To provide maximum throughput between 3100 and 4000 Å, we used a 400 groove mm<sup>-1</sup> grism blazed at 3400 Å on LRIS-B, resulting in a dispersion of 1.09 Å per pixel. For simultaneous observations on the red-side of LRIS (LRIS-R), we used a 400 groove mm<sup>-1</sup> grating blazed at 8500 Å, providing wavelength coverage up to 9500 Å. We typically obtained simultaneous blue and red side spectroscopic observations between 3100 and 9500 Å, with slight variations due to the relative placement of slits in the telescope focal plane.

The slit masks used for spectroscopy cover  $8' \times 5'$  on the sky. For a minimum slit length of 9'' (adopted in order to ensure good background subtraction), we are able to include 30–35 slits, in addition to 4–5 star boxes used to accurately align each mask. We set the width of each slit to 1''.2 and this, combined with a typical seeing of 0''.8, yields a typical resolution of 5 Å for point sources. To obtain the optimum mix of objects on any given slit mask, we assigned each candidate a weight primarily based on its optical magnitude. We gave larger weights to objects with  $\mathcal{R} = 23.5 - 24.5$  and lower weights for fainter objects where absorption line spectroscopy is more difficult and brighter objects where the foreground ( $z \lesssim 1.0$ ) interloper fraction is larger. Nonetheless, we filled “blank” areas of the masks with filler objects which included these fainter and brighter objects. In particular, we included some bright ( $\mathcal{R} < 23.5$ ) objects on masks since at least some of these are intrinsically bright  $z \sim 2 - 3$  galaxies and are most suitable for detailed followup spectroscopic studies. To support other projects being conducted by our group, we also deliberately targeted objects within the  $U_nGR$  sample that had interesting multi-wavelength properties, such as those identified with 850 μm or 24 μm emission, as well as those with unusually red near-IR col-

ors. We also designed masks to overlap as much as possible with the near-IR imaging. Because of this,  $\sim 73\%$  of spectroscopically confirmed galaxies with  $z > 1.4$  lie in the  $K_s$ -band region, even though  $\sim 50\%$  of  $U_nGR$  candidates lie in the same region (see Figure 1).

We typically obtained 3 exposures of 1800 sec per mask, for a total exposure of 5400 sec. The range in optical magnitudes implies a large range in the S/N of the spectra. At the minimum, however, we found 5400 sec to be sufficient to obtain redshifts, and a few objects were observed on more than one mask. The spectroscopic success rate per mask is primarily a function of the weather conditions (e.g., cirrus, seeing) at the time of observation, with a 90% success rate of obtaining redshifts in the best conditions; these redshifts, for the most part, fell within the targeted redshift ranges. This suggests that the redshift distribution for the spectroscopic and photometric samples are similar, and there are not large numbers of galaxies whose true redshifts are far from those expected based on their observed  $U_nGR$  colors. Details of the spectral reduction techniques are described in Steidel et al. (2003). We identified redshifts based on the presence of a number of low-ionization interstellar absorption lines (e.g., Si II λ1260, O I+S II λ1303, C II λ1334, Si II λ1526, Fe II λ1608, Al II λ1670, and Al III λ1854, 1862), stellar wind features (e.g., N V λ1238, 1242, S IV λ1393, 1402, and C IV λ1548, 1550), the C III λ1909 nebular emission line, or Lyα emission or absorption. A few examples of spectra are shown in Steidel et al. (2003, 2004). Spectroscopically confirmed galaxies with  $1.4 < z < 3.0$  are shown with respect to the  $\mathcal{R}$ -band image of the GOODS-N field in Figure 1.

Comparison with nebular redshifts derived from Hα spectroscopy indicates that Lyα emission is almost always redshifted, and interstellar absorption lines are almost always blueshifted, with respect to the systemic (nebular) redshift of the galaxy. These systematic offsets have been interpreted as the result of outflows (e.g., Adelberger et al. 2003, 2005b; Pettini et al. 2001; Shapley et al. 2003). Adelberger et al. (2005b) present linear least-squares fits to the systemic redshifts of galaxies given their Lyα and interstellar absorption redshifts based on a sample of 138 objects with near-IR spectroscopy (Erb et al. 2006c; Pettini et al. 2001).

### 3. SPECTROSCOPIC RESULTS AND CATALOG

Our spectroscopic sample in the GOODS-N field presently includes 212 BM/BX and 74 C/D/MD galaxies with secure spectroscopic redshifts  $z > 1.4$  (Table 2). The total sample includes 347 objects with secure spectroscopic redshifts, including 40 interlopers with  $z < 1$ . We also include 41 objects with uncertain redshifts in Table 2, denoted by a colon (“:”) in the redshift field (for consistency with Steidel et al. 2003), for a total of 388 objects. Table 1 lists the statistics for the individual samples, including the numbers of candidates observed, the interloper fractions, and mean redshifts. The primary source of contamination in the LBG sample is from K dwarfs in the Galactic halo. Star-forming galaxies at redshift  $\langle z \rangle = 0.17 \pm 0.09$  contaminate the BX sample since their Balmer breaks mimic the Lyα forest decrement. These interlopers can be easily excluded using  $K_s$ -band photometry (e.g., the  $BzK$  criteria; Daddi et al. 2004), but we have not imposed any additional criteria

other than the observed optical magnitudes and colors. The main “contaminants” of the BM sample occur from galaxies with redshifts  $1.0 < z < 1.4$ ; these galaxies have  $U_nGR$  colors very similar to those of BM objects, and the narrow BM color selection window implies that photometric scatter and Ly $\alpha$  perturbations on the  $U_nGR$  colors can have a significant impact on the observed redshift distribution of BM galaxies (Reddy et al., in prep.). Throughout this paper we consider objects with  $z < 1.4$  to be contaminants. The AGN/QSO (as identified from either their X-ray, UV, or *Spitzer* IRAC or MIPS emission) with  $z > 1.4$  make up  $\sim 4\%$  of the sample (see § 6.2 for further discussion).

For consistency, we compared redshifts for objects in common with the Team Keck Treasury Redshift Survey (TKRS; Wirth et al. 2004; Cowie et al. 2004). We note that the TKRS survey is based primarily upon observations with the DEIMOS instrument on Keck II, and so the TKRS redshift selection function rapidly declines above  $z \sim 1.2$  as the emission and absorption lines used for redshift identification (including [N II], [S II], [O III], [O II] emission features and Calcium H and K absorption features) are shifted out of the DEIMOS spectral range. The overlap between the  $U_nGR$  and TKRS samples is small given that the two surveys target different redshifts (TKRS is better at identifying galaxies at  $z \lesssim 1.2$  and our  $U_nGR$  selection is better at identifying galaxies at  $z \gtrsim 1.4$ ).

There are 64 objects with redshifts in the  $U_nGR$  catalog which are also in the TKRS database. Of these, 52 were previously published in other surveys of the GOODS field (Cowie et al. 2004; Cohen et al. 1996, 2000; Cohen 2001; Barger et al. 2000, 2003; Wirth et al. 2004; Phillips et al. 1997; Lowenthal et al. 1997; Dawson et al. 2001; Steidel et al. 2003, 1996; Dickinson 1998) and/or have agreement in redshift between the  $U_nGR$  and TKRS samples. Upon further inspection of the 12 objects with discrepant redshifts, we adopted the TKRS redshift for 6 of them (BX1202, BX1371, BMZ1010, BMZ1100, BMZ1121, and BMZ1208); the redshifts for these 6 galaxies are all below  $z < 1.4$  where the DEIMOS-determination was found to be secure and where our BM selection function drops off. Five of the objects had the correct redshifts in our catalog (BX1299, BX1319, BX1805, BMZ1119, and BMZ1375). For the remaining object, BX1214, we were able to rule out the Cohen et al. (2000) redshift of  $z = 2.500$ , but were unable to confidently assign a redshift based on our LRIS spectrum.

The redshift distributions of BM/BX and LBG galaxies with  $z_{\text{spec}} > 1$  are shown in Figure 3, where the right panel emphasizes large-scale structure in the GOODS-N field. The redshift over-density at  $z = 2.95$  is prominent, and was also noted in the LBG survey (Steidel et al. 2003). We also note a possible over-density at  $z = 2.00$ , which corresponds to an over-density of 5 submillimeter galaxies as noted by Blain et al. (2004). However, we caution that Figure 3 only presents raw numbers, and we have not accounted for the selection function and relative fractions of candidates observed. Therefore, the significance of any redshift “over-densities” appearing in Figure 3 is not quantified.

#### 4. SPITZER IRAC AND MIPS DATA

To aid in understanding the stellar populations and extinction of  $z \sim 2$  galaxies, we compiled *Spitzer* IRAC and MIPS photometry for our sample of  $U_nGR$ -selected galaxies using the public *Spitzer* data in the GOODS-N field (Dickinson et al., in prep; Chary et al., in prep). The IRAC photometry was performed by fitting an empirical point spread function (PSF) determined from the IRAC images to the spatial positions of sources from the higher resolution  $K_s$ -band data. Specifically, to accurately compute the empirical PSF for each IRAC channel we used as many isolated point sources located throughout the IRAC images as possible. Changing the number of objects used to compute the PSF results in variations of the best-fit fluxes of  $< 5\%$ , and is generally small compared to the background noise (see below). Using the  $K_s$ -band data to constrain source positions mitigates the effects of confusion by allowing for the deblending of partially resolved sources in the IRAC images, and is similar to the method employed by the GOODS team for extracting photometry (Dickinson et al., in prep; Chary et al., in prep; see also Labb   et al. 2005 and Shapley et al. 2005). We extracted the MIPS 24  $\mu\text{m}$  fluxes of  $U_nGR$  galaxies using a similar procedure; the spatial positions of sources from the IRAC data were used to deblend and extract the 24  $\mu\text{m}$  fluxes (Reddy et al. 2006). Errors for both IRAC and MIPS photometry were computed from the dispersion of extracted fluxes for 100 PSFs fit to random blank regions around each galaxy. Since the IRAC and MIPS data are background-limited, the errors will be dominated by the background noise for all but the brightest galaxies at these wavelengths. The IRAC channel 1 – 4 magnitudes and MIPS 24  $\mu\text{m}$  fluxes are listed in Table 2.<sup>9</sup> We do not give fluxes for those galaxies which were either undetected or were badly blended with a nearby bright source. Of the 212 BX/BM galaxies with secure spectroscopic redshifts  $z > 1.4$ , only 2 ( $< 1\%$ ) are undetected at 3.6  $\mu\text{m}$  to the GOODS IRAC depth. Of the 74 LBGs, 11 ( $\approx 15\%$ ) are undetected at 3.6  $\mu\text{m}$ . The MIPS detection fraction is  $\approx 65\%$  for BX/BM galaxies, decreasing to  $\approx 53\%$  for the LBGs, to a limiting 3  $\sigma$  flux of  $f_{24\mu\text{m}} \approx 8 \mu\text{Jy}$ .

#### 5. STELLAR POPULATION MODELING

The combination of multi-wavelength photometry and spectroscopic redshifts allows us to better constrain the stellar populations of UV-selected galaxies than if we only had photometric redshifts. To demonstrate the wide range in stellar populations of UV-selected galaxies at redshifts  $z \sim 2 - 3$ , we fit the  $U_nGRJK_s$  + IRAC magnitudes with Bruzual & Charlot (2003) models assuming a Salpeter (1955) IMF and solar metallicity. The assumption of solar metallicity is a reasonable approximation for most galaxies in the  $U_nGR$ -selected sample (Erb et al. 2006a). The models were corrected for the effects of IGM opacity before comparing to the observed magnitudes. In fitting the stellar populations, we assumed an exponentially-declining star formation history with decay time scales  $\tau = 10, 20, 50, 100, 200, 500, 1000, 2000$ , and 5000 Myr, and  $\tau = \infty$  (constant star formation, CSF, model). We also assumed a varying amount of reddening, or  $E(B - V)$ , from 0.0 to 0.7. The best-

<sup>9</sup> Magnitude and flux errors for the *Spitzer* data are provided in the accompanying machine-readable table.

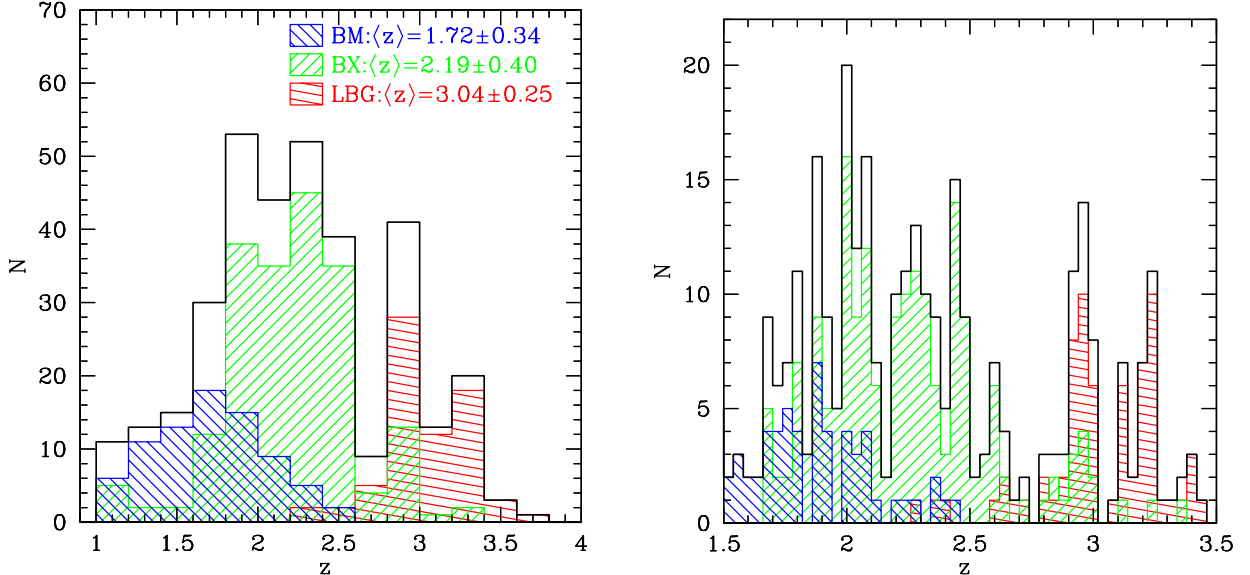


FIG. 3.— (Left) Redshift histogram of spectroscopically confirmed BM/BX and LBG galaxies in the GOODS-N field with  $z > 1$ . The solid line indicates the total distribution of BM, BX, and LBG galaxies. (Right) Redshift histogram with higher resolution bins,  $\delta z = 0.04$ , emphasizing large-scale structure in GOODS-N.

fit model was taken to be the combination of  $\tau$ , age, and  $E(B - V)$  that gave the lowest  $\chi^2$  value with respect to the observed magnitudes. The star formation rate (SFR) and stellar mass are determined from the normalization of the model to the observed magnitudes. Even with spectroscopic redshifts, there is considerable uncertainty in the best-fit parameters, with the exception of the total stellar mass  $M^*$  which is generally robust to changes in the assumed star formation history (e.g., Papovich et al. 2001; Shapley et al. 2001; Sawicki & Yee 1998; Shapley et al. 2005; Erb et al. 2006c). The best-fit stellar population parameters for both a CSF and  $\tau$  model for each galaxy are collected in Table 3. Monte Carlo simulations indicate that the typical fractional uncertainties associated with the best-fit parameters (when including IRAC data in the fits) are  $\langle \sigma_x / \langle x \rangle \rangle = 0.6, 0.4, 0.5,$  and  $0.2$  in  $E(B - V)$ , age, SFR, and stellar mass, respectively (Erb et al. 2006c). For completeness we have included the best-fit SFRs from the fitting in Table 3, but we note that we have several other *independent* multi-wavelength measures of the SFRs for these galaxies (e.g., from dust-corrected UV, H $\alpha$ , and 24  $\mu\text{m}$  data) that are unaffected by the degeneracies associated with stellar population modeling.

Aside from the systematic errors resulting from the degeneracy between star formation history and the best-fit parameters, there are additional caveats to the SED results. Around 30 objects had optical through IRAC photometry which is inconsistent with the stellar population models considered here; these objects exhibit large  $J/K_s$  and IRAC magnitude residuals with respect to the best-fit stellar population (and have  $\chi^2 > 10$ ), and often give unrealistically young ages ( $< 10$  Myr) and large SFRs ( $> 2000 M_\odot \text{ yr}^{-1}$ ). We do not present the SED results for these galaxies. In addition to these 30, there are 4 galaxies which fit the optical and IRAC data well, but have large  $K_s$  residuals with respect to the best-fit stellar population (i.e., a  $K_s$  magnitude more than  $3\sigma$  away from the best-fit). Three of these 4 galaxies have redshifts  $2.0 \leq z \leq 2.5$  where the  $K_s$  magnitude

may be contaminated by emission from H $\alpha$ +[N II]. The 4 galaxies with large  $K_s$  residuals are indicated by the notation “ $K_s$ ” in Table 3. Also, we noted a few objects with 8  $\mu\text{m}$  excesses when compared with the best-fit stellar population, many of which have large 24  $\mu\text{m}$  fluxes ( $f_{24\mu\text{m}} > 100 \mu\text{Jy}$ ) indicating they may be obscured AGN (see Table 5). We do not present SED fitting results for any of the sources which may have AGN based on their 8  $\mu\text{m}$  and 24  $\mu\text{m}$  excesses and/or X-ray/optical emission. Finally, we did not perform SED fitting for galaxies without photometry longward of R-band or which had redshifts  $z < 1$ . The best-fit SED parameters for the remaining 254 galaxies are listed in Table 3. Note that the SFRs and stellar masses ( $M^*$ ) in Table 3 assume a Salpeter (1955) IMF from 0.1 to 100  $M_\odot$ . Assuming the Chabrier (2003) IMF with a shallower faint-end slope results in SFRs and stellar masses a factor of 1.8 lower than listed in Table 3. We also note that a number of galaxies have inferred ages  $< 50$  Myr, which are unlikely given the dynamical time-scale of  $\sim 50$  Myr for star formation in galaxy-sized objects. The SED parameters for these galaxies with extremely young *inferred* ages should be taken with caution.

## 6. THE DIVERSE PROPERTIES OF OPTICALLY-SELECTED GALAXIES AT HIGH REDSHIFT

### 6.1. Star-Forming Galaxies

Of the best-fit SED parameters, the stellar mass is the least uncertain and is generally robust to changes in the assumed star formation history, as can be seen by comparing columns 6 and 11 in Table 3. Figure 4 shows the distribution of stellar masses for  $U_nG\mathcal{R}$ -selected galaxies with redshifts  $z > 1$ , assuming a constant star formation history. Table 4 shows the median and mean stellar masses and dispersion (assuming a CSF history) for galaxies in the various samples. While the mean stellar mass of the sample is  $\langle M^* \rangle \approx 1.1 \times 10^{10} M_\odot$ , there is large dispersion about this mean of a factor of 3.4. This mean stellar mass is a factor of  $\sim 2$  lower than found in Shapley et al. (2005) and Erb et al. (2006c), partly be-

cause we included galaxies undetected to  $K_s = 24.1$  in the sample considered here (as long as they had IRAC data to constrain the stellar mass), and these faint  $K_s$  galaxies on average have lower stellar masses than  $K_s$ -detected galaxies. Further, we have included BM galaxies which have a mean stellar mass that is a factor of  $\approx 2$  lower than the mean stellar mass for BX galaxies and LBGs (Table 4). This difference in mean stellar mass likely reflects the fact that BM galaxies have a lower mean redshift ( $z = 1.72 \pm 0.32$ ; Figure 3) than BX galaxies and LBGs, and therefore we are able to probe down to fainter absolute magnitudes and are sensitive to lower mass galaxies.

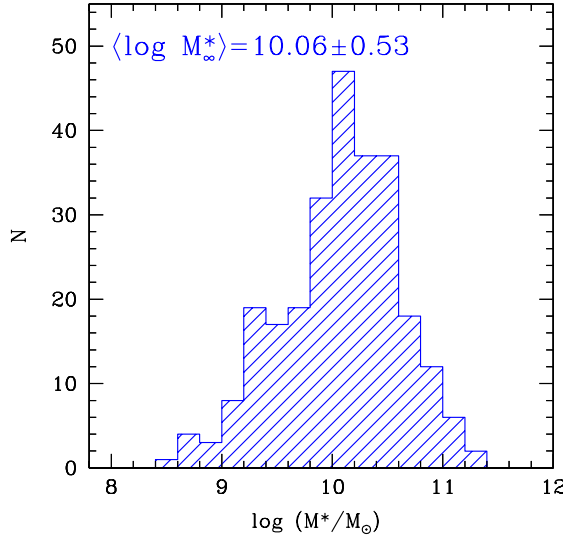


FIG. 4.— Stellar mass distribution of  $U_nGR$ -selected galaxies with redshifts  $z > 1$ , assuming a constant star formation (CSF) model. Assuming a best-fit exponentially declining star formation history ( $\tau$  model) results in a stellar mass distribution that is virtually identical to the one shown here, with a mean and dispersion in log space of  $\langle \log M^* \rangle = 10.08 \pm 0.51$ .

Regardless, the sample includes galaxies with a wide range in ages, from young galaxies with ages comparable to the dynamical timescale for star formation of  $\sim 50$  Myr to those which are older than 2 Gyr. In fact, the  $U_nGR$  sample includes galaxies which are as old ( $> 2$  Gyr) and as massive ( $M^* > 10^{11} M_\odot$ ) as galaxies found at  $z \sim 2$  in near-IR selected samples (e.g., the distant red galaxies, or DRGs, of Franx et al. 2003)<sup>10</sup>. In particular, Shapley et al. (2005) and Reddy et al. (2005) have shown that while the typical stellar mass of near-IR selected DRGs with  $K_s \lesssim 21.8$  is larger by an order of magnitude than the typical stellar mass of  $U_nGR$ -selected galaxies to  $R = 25.5$ , the actual range in stellar mass probed by DRG selection does not appear to significantly exceed the range in stellar mass of  $U_nGR$ -selected galaxies (although we note that DRG selection appears to be much more efficient in selecting galaxies with  $M^* \gtrsim 10^{11} M_\odot$  at  $z \sim 2-3$ ; e.g., van Dokkum et al. 2006). Further, SED analysis of the optically-selected DRGs (as indicated in Table 2 by the notation “DRG” in the last column) with fainter near-IR magnitudes

<sup>10</sup> Optically selected galaxies which satisfy the DRG criteria ( $J - K_s > 2.3$  in Vega magnitudes, or  $J - K_s > 1.38$  in AB) are indicated by “DRG” in the last column of Table 2. There are 19 such DRGs with secure spectroscopic redshifts in our sample.

( $K_s \gtrsim 22.8$ ) have stellar masses that are comparable to the stellar masses of typical  $U_nGR$ -selected galaxies ( $10^9 \lesssim M^* \lesssim 10^{11} M_\odot$ ). While optical selection allows us to very efficiently followup galaxies spanning over two orders of magnitude in age and stellar mass at redshifts  $z \gtrsim 1.4$ , other techniques are required to assess the total stellar mass budget at these redshifts (e.g., Rudnick et al. 2006; van Dokkum et al. 2006; Reddy et al. 2005).

While the  $E(B - V)$  and SFRs determined from SED modeling are more uncertain than the inferred stellar masses, we have several independent methods of assessing the extinction and SFRs in  $z \sim 2$  galaxies, made possible by the extensive multi-wavelength data in the GOODS-N field. The exquisite, photon-limited *Chandra* X-ray data in the GOODS-N field, currently the deepest X-ray data ever taken (Alexander et al. 2003), allow for stacking analyses to estimate the average emission properties of galaxies (Brandt et al. 2001; Nandra et al. 2002; Reddy & Steidel 2004; Reddy et al. 2005). Based on the stacking analyses of Nandra et al. (2002) and Reddy & Steidel (2004), the mean SFRs of  $z \sim 2-3$   $U_nGR$ -selected galaxies is  $\sim 50 M_\odot \text{ yr}^{-1}$ , with mean attenuation factors, defined as the ratio between the bolometric SFR and UV-based SFR (uncorrected for extinction), of  $4.5 - 5.0$ .

The X-ray data allow us to determine the average extinction and SFRs of galaxies over the entire range of redshifts probed by the BX/BM and LBG criteria. However, important progress has been made in determining the individual properties of galaxies in a narrower redshift range,  $1.5 \lesssim z \lesssim 2.6$ , where the *Spitzer* MIPS  $24 \mu\text{m}$  band is sensitive to the  $7.7 \mu\text{m}$  polycyclic aromatic hydrocarbon (PAH) dust emission ubiquitous in local and high redshift star forming galaxies (Reddy et al. 2006; Papovich et al. 2006). Reddy et al. (2006) demonstrate that the  $24 \mu\text{m}$  emission of  $z \sim 2$  galaxies can be used as a tracer of the SFR or total infrared luminosity ( $L_{\text{IR}}$ ), particularly for galaxies with spectroscopic redshifts where we are able to accurately constrain the  $K$ -corrections from  $24 \mu\text{m}$  flux to rest-frame  $5-8.5 \mu\text{m}$  luminosity. The MIPS data indicate that  $U_nGR$ -selected galaxies at redshifts  $1.5 \lesssim z \lesssim 2.6$  span more than 3 orders of magnitude in  $L_{\text{IR}}$ , from those which are undetected to the  $3\sigma$  sensitivity limit of  $8 \mu\text{Jy}$  for MIPS data in the GOODS field, to those which have  $L_{\text{IR}}$  comparable to the most luminous star-forming galaxies at these redshifts, the submillimeter galaxies (Smail et al. 1997; Hughes et al. 1998; Barger et al. 1998; Chapman et al. 2005). The mean infrared luminosity for  $U_nGR$ -selected galaxies is  $\langle L_{\text{IR}} \rangle \simeq 2 \times 10^{11} L_\odot$ , assuming that the rest-frame infrared emission ( $L_{5-8.5\mu\text{m}}$ ) as probed by MIPS observations scales with infrared luminosity as  $L_{\text{IR}} \approx 17.2 L_{5-8.5\mu\text{m}}$  as determined from local samples (see Reddy et al. 2006), and this value of  $\langle L_{\text{IR}} \rangle$  inferred from MIPS is in excellent agreement with X-ray and dust-corrected UV-based estimates. Reddy et al. (2006) further demonstrate that the agreement in SFR extends to galaxies on an individual (object-by-object) basis for a small sample of  $U_nGR$ -selected galaxies with both  $24 \mu\text{m}$  and  $H\alpha$  detections: the scatter between the bolometric luminosity inferred from  $24 \mu\text{m}$  versus  $H\alpha$  observations is  $\sim 0.2$  dex. Finally, we have compared the  $24 \mu\text{m}$ -estimated SFRs with those obtained from the SED-fitting analysis: as expected they are positively cor-

related at the  $5\sigma$  level with a scatter of 0.3 dex assuming a CSF model.<sup>11</sup> The advantage of multi-wavelength data is that we can assess SFRs independent of the degeneracies associated with SED-fitting. In summary, the  $U_nGR$ -selected sample includes galaxies over 4 orders of magnitude in dust obscuration ( $L_{\text{bol}}/L_{\text{UV}}$ ), from those galaxies with little dust and whose UV luminosity is comparable to  $L_{\text{IR}}$ , to those which are heavily dust-obscured and have attenuation factors  $\gtrsim 1000$ .

Aside from the large dynamic range in SFRs and extinction of  $U_nGR$ -selected galaxies, the sample also hosts galaxies with a wide range in morphology and kinematics (Erb et al. 2003, 2006c; Law et al., in prep.), from disk-like galaxies with signatures of rotation, as inferred from H $\alpha$  spectral data (e.g., Forster Schreiber et al. 2006), to those galaxies which appear irregular and/or are merging. UV-selected samples efficiently target the redshift range where the morphological transformation of galaxies from irregular at high redshift to the Hubble sequence at low redshifts ( $z \lesssim 1.4$ ) takes place. The deep Hubble ACS data in the GOODS field (Giavalisco et al. 2004) combined with our extensive rest-frame UV spectroscopic database make it possible to study in detail the correlation between morphological structure and the SFRs, extinction, masses, and spectral properties of high redshift galaxies (Law et al., in prep.).

## 6.2. AGN

The combination of X-ray, observed optical, 8  $\mu\text{m}$ , and 24  $\mu\text{m}$  data, along with spectroscopic redshifts, allows for a powerful probe of AGN activity among  $U_nGR$ -selected galaxies. We classified objects as AGN based on one or more of the following criteria: (a) the presence of high ionization UV lines (identical to the method used in Steidel et al. 2002 and Shapley et al. 2005); (b) direct detection in the *Chandra* 2 Ms data (Alexander et al. 2003) and an X-ray-to-optical flux ratio indicative of AGN (e.g., see Hornschemeier et al. 2001 and Reddy et al. 2005); or (c) an 8 and 24  $\mu\text{m}$  flux excess above what one would expect from a simple star-forming population. Table 5 lists the 11 AGN with confirmed redshifts  $z > 1.4$  which have emission indicative of AGN.

MD31 is the most unusual source: it has an X-ray counterpart within 1''.5 of the optical position, but shows no evidence of AGN from the rest-UV (observed optical) spectrum nor from *Spitzer* observations. The SED analysis indicates that MD31 is best-fit with an  $\sim 2$  Gyr old population with a modest  $E(B - V) \sim 0.17$  and  $\text{SFR} \sim 60 \text{ M}_\odot \text{ yr}^{-1}$  assuming the CSF model, and thus is not expected to be bright in X-rays as a result of star formation alone (i.e., the 2 Ms X-ray sensitivity implies a detection threshold of  $\sim 480 \text{ M}_\odot \text{ yr}^{-1}$  at the redshift of MD31,  $z = 2.981$ ). Examination of the deep ACS imaging in the GOODS field reveals no other optical counterpart within 1''.5 of MD31. If the X-ray counterpart is indeed associated with accretion activity in MD31, then the X-ray detection fraction of AGN with  $z > 1.4$  in our sample is 7/11, or 64%. On the other hand, the fraction

of AGN showing 8  $\mu\text{m}$  and/or 24  $\mu\text{m}$  excesses is 9/11, or 82%. While the object statistics are insufficient to judge the efficiency of AGN detection in the X-ray versus IR, we note that the IRAC and MIPS integration time for any given object in the GOODS-N field is  $\sim 10$  hours, whereas the X-ray integrations required to detect faint AGN at redshifts  $z \gtrsim 1.4$  is on the order of a megasecond or larger. The possible difference in AGN detection fraction and especially integration time between the IR and X-ray observations suggest that deep IR imaging may be a more efficient method of finding AGN at high redshifts. In this case, the 8  $\mu\text{m}$  and 24  $\mu\text{m}$  data indicate at least an additional 3 AGN which are unidentified in X-rays. For comparison, while our optical spectra have integration times of 5400 s, a factor of 370 times shorter than the X-ray integration time (2 Ms), we can still detect  $\approx 73\%$  of AGN based on their rest-frame UV emission lines.

The properties of the 3 X-ray undetected AGN with  $z > 2$  are worth further consideration: these AGN are BX1637, BX160, and MD74. Figure 5 shows the observed optical through 24  $\mu\text{m}$  SEDs of these AGN, as well as BM1156 which is very weakly detected in X-rays, and demonstrates the power-law behavior at observed wavelengths longer than  $\lambda \sim 2 \mu\text{m}$ , indicative of warm dust population. The three X-ray undetected AGN are also not detected in the deep radio imaging of the HDF (Richards 2000), placing a  $3\sigma$  upper limit on their observed 1.4 GHz flux of  $f_{1.4 \text{ GHz}} < 24 \mu\text{Jy}$ . However, all three have disturbed and/or extended rest-frame UV morphologies from deep ACS imaging (Giavalisco et al. 2004), suggesting the obscured AGN in these systems may be triggered by merger activity. The non-detection of these three AGN (even when stacking them) in both the soft (0.5 – 2.0 keV) and full (2.0 – 8.0 keV) X-ray bands of *Chandra* makes it difficult to constrain their column densities. Nonetheless, these three AGN have a mean spectroscopic redshift of  $\langle z_{\text{AGN}} \rangle \approx 2.5$ , and if we assume the AGN have intrinsic photon index of  $\Gamma = 2.0$  (e.g., Alexander et al. 2005), then we cannot rule out the possibility that these could be Compton-thick AGN with column densities  $N_{\text{H}} > 10^{24} \text{ cm}^{-2}$ . Comparison with the 8  $\mu\text{m}$  and 24  $\mu\text{m}$  fluxes of Mrk 463 and Mrk 1014, two infrared luminous AGN (Armus et al. 2004), suggests that BX1637 and MD74 could have total infrared luminosities in the range  $5 \times 10^{12} \lesssim L_{\text{IR}} \lesssim 2 \times 10^{13} \text{ L}_\odot$ . Constraints on the 850  $\mu\text{m}$  fluxes of these two AGN could narrow the range of possible  $L_{\text{IR}}$ , but unfortunately submillimeter observations do not cover the region containing these two AGN. BX160 is covered in published 850  $\mu\text{m}$  imaging and is undetected to  $S_{850} \sim 1.5 \text{ mJy}$  (Wang et al. 2004), suggesting an upper limit on the infrared luminosity of  $\sim 10^{12.5} \text{ L}_\odot$ . We caution, however, that the lack of data across the Raleigh-Jeans tail of the dust SEDs makes it difficult to accurately constrain the dust temperatures and hence total bolometric luminosities of these sources.

The presence of obscured AGN at high redshifts has been postulated based on the expected fraction of high column density AGN ( $N_{\text{H}} > 10^{23} \text{ cm}^{-2}$ ) at  $z \gtrsim 1.4$  in simulations that model the contribution to the X-ray background (Comastri & Fiore 2004; Gilli 2004). While high column density AGN may be unidentifiable as AGN based on their optical spectra alone, the fact that some fraction of their host galaxies are optically bright ( $\mathcal{R} < 25.5$ ) and fall within optically-selected sam-

<sup>11</sup> Adopting a declining model, as opposed to assuming a CSF model for all galaxies, will generally increase the scatter in SFRs since the youngest galaxies will have inferred SFRs (from declining star formation history models) that are systematically lower than those inferred from H $\alpha$  observations (see discussion in Erb et al. 2006b).

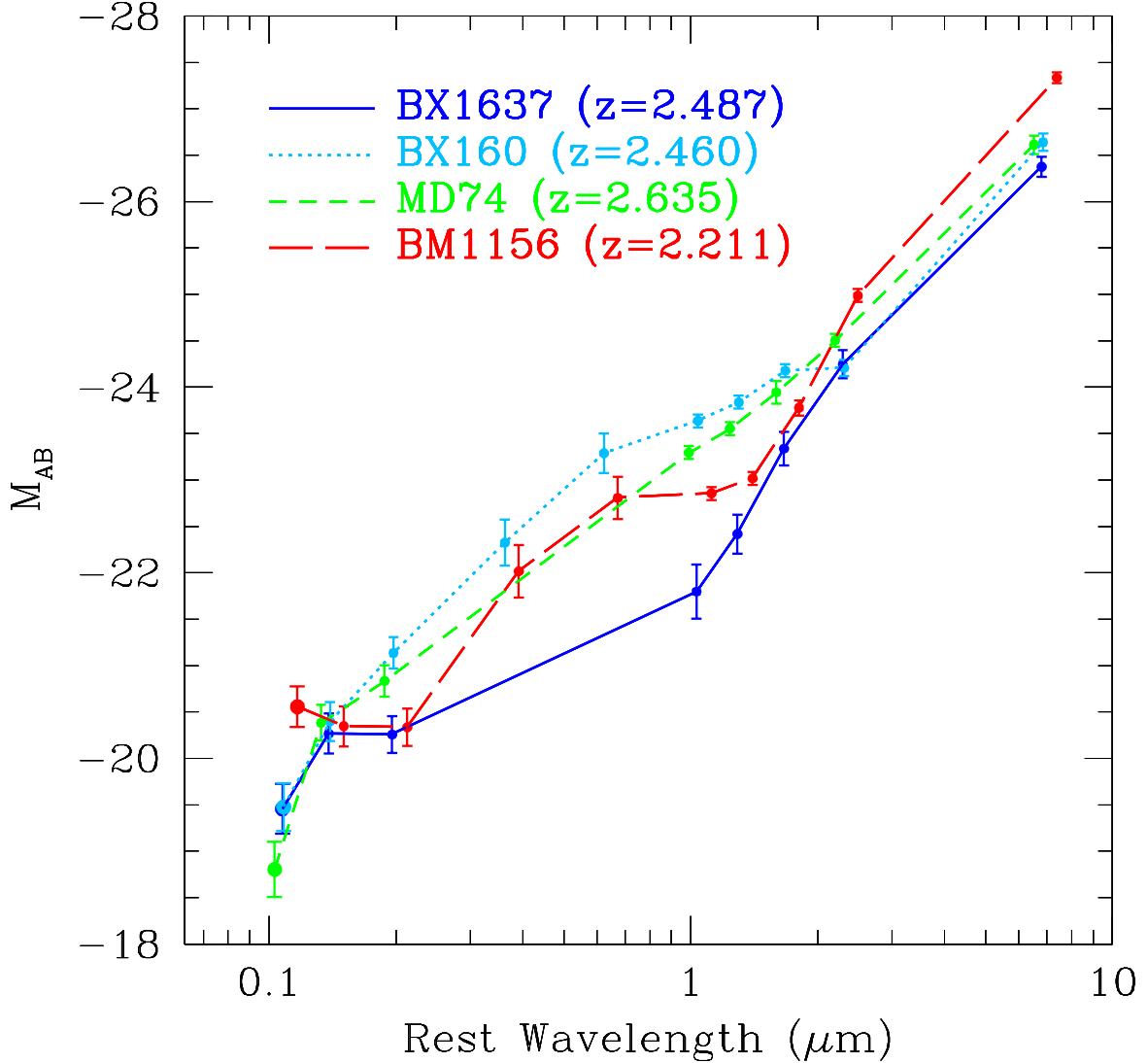


FIG. 5.— Spectral energy distributions of the three X-ray undetected AGN (BX1637, BX160, and MD74) and one faint X-ray detected AGN (BM1156) at  $z = 2.211 - 2.635$  in the spectroscopic  $U_nGR$  sample, from observed optical through  $24\ \mu\text{m}$ . All four exhibit a power law slope at long wavelengths ( $\lambda \gtrsim 2\ \mu\text{m}$  rest-frame) indicative of a warm dust population.

ples bodes well for determining their spectroscopic redshifts. Accurate spectroscopic redshifts are particularly important for constraining AGN column densities ( $N_{\text{H}}$ ); the inferred  $N_{\text{H}}$  depends strongly on the assumed redshift,  $N_{\text{H}}(z) \approx N_{\text{H}}(0)(1+z)^{2.6}$  (Alexander et al. 2005).

In summary, of the 11 AGN with  $z > 1.4$  in our optically-selected sample, 7/11 (64%) are detected in X-rays to 2 Ms, 9/11 (82%) are detected with 8 and/or  $24\ \mu\text{m}$  excesses, and 8/11 (73%) have rest-frame UV signatures of AGN. Even in the deepest X-ray image available, there is still a considerable number of AGN that remain undetected, and we must incorporate other techniques, e.g., optical spectra and 8 and  $24\ \mu\text{m}$  data, to fully account for the census of AGN.

## 7. SUMMARY

We have presented the results of a spectroscopic survey of redshift  $1.4 \lesssim z \lesssim 3.0$  star-forming galaxies in the GOODS-North field, made possible by efficient UV ( $U_nGR$ ) color selection and the unique multi-object capabilities of the LRIS instrument on the Keck I telescope. Our sample consists of 212 redshifts for galaxies at red-

shifts  $1.4 \lesssim z \lesssim 2.5$  selected using the BM and BX criteria of Adelberger et al. (2004) and Steidel et al. (2004), and 30 new redshifts (of a total of 74) for Lyman break galaxies at redshifts  $2.5 \lesssim z \lesssim 3.5$ . Our deep optical and near-IR imaging, supplemented by publicly available *Spitzer* IRAC and MIPS data (Dickinson et al., in prep; Chary et al., in prep), allow us to measure the stellar populations, stellar masses, star formation rates, and dust extinction for galaxies in our sample (e.g., Erb et al. 2006c; Shapley et al. 2003, 2005; Reddy & Steidel 2004; Reddy et al. 2005, 2006; Steidel et al. 2004). These analyses indicate that the  $U_nGR$ -selected sample consists of galaxies which span two orders of magnitude in age and stellar mass, and 4 orders of magnitude in dust obscuration ( $L_{\text{bol}}/L_{\text{UV}}$ ). Included are galaxies with bolometric star formation rates ranging from  $\sim 5\ M_{\odot}\ \text{yr}^{-1}$  to  $> 1000\ M_{\odot}\ \text{yr}^{-1}$ . We further identify at least 3 of 11 AGN in our sample which appear to be heavily dust-obscured based on their power-law SEDs longward of  $2\ \mu\text{m}$  (rest-frame) and lack of detection in the deep *Chandra* 2 Ms data (Alexander et al. 2003). A compilation of the multi-wavelength data for these 11 AGN indicates

that optical and *Spitzer* data are able to more efficiently (in terms of integration time) select AGN at  $z > 1.4$  than X-ray data, but optical spectra and *Spitzer* and *Chandra* data are all required to fully account for the census of AGN at high redshifts. The photometry and SED fitting results for galaxies in our sample are available at <http://www.astro.caltech.edu/~drlaw/GOODS/>.

Large spectroscopic samples at high redshifts allow for a number of other detailed investigations such as the galaxy and AGN/QSO luminosity functions (Steidel et al. 1999; Adelberger & Steidel 2000; Shapley et al. 2001; Hunt et al. 2004, Reddy et al. in prep.); metallicities (Pettini et al. 1998, 2001; Shapley et al. 2004; Erb et al. 2006a); signatures of galaxy feedback and IGM metal enrichment

(Adelberger et al. 2003); and accurate clustering analyses (Adelberger et al. 2005a,b). This large range in galaxy evolution studies highlights the versatility and efficiency of optically-selected samples in addressing many fundamental issues in cosmology.

We thank David Law for setting up the website where the galaxy photometry and SED fits are available to the public. We are grateful to the staff of the Keck and Palomar Observatories for their help in obtaining the data presented here. This work has been supported by grant AST 03-07263 from the National Science Foundation and by the David and Lucile Packard Foundation.

## REFERENCES

- Adelberger, K. L., Erb, D. K., Steidel, C. C., Reddy, N. A., Pettini, M., & Shapley, A. E. 2005a, ApJ, 620, L75  
 Adelberger, K. L., Shapley, A. E., Steidel, C. C., Pettini, M., Erb, D. K., & Reddy, N. A. 2005b, ApJ, 629, 636  
 Adelberger, K. L. & Steidel, C. C. 2000, ApJ, 544, 218  
 Adelberger, K. L., Steidel, C. C., Shapley, A. E., Hunt, M. P., Erb, D. K., Reddy, N. A., & Pettini, M. 2004, ApJ, 607, 226  
 Adelberger, K. L., Steidel, C. C., Shapley, A. E., & Pettini, M. 2003, ApJ, 584, 45  
 Alexander, D. M. et al. 2003, AJ, 126, 539  
 Alexander, D. M., Bauer, F. E., Chapman, S. C., Smail, I., Blain, A. W., Brandt, W. N., & Ivison, R. J. 2005, ApJ, 632, 736  
 Armus, L. et al. 2004, ApJS, 154, 178  
 Barger, A. J., Cowie, L. L., Capak, P., Alexander, D. M., Bauer, F. E., Fernandez, E., Brandt, W. N., Garmire, G. P., & Hornschemeier, A. E. 2003, AJ, 126, 632  
 Barger, A. J., Cowie, L. L., & Richards, E. A. 2000, AJ, 119, 2092  
 Barger, A. J., Cowie, L. L., Sanders, D. B., Fulton, E., Taniguchi, Y., Sato, Y., Kawara, K., & Okuda, H. 1998, Nature, 394, 248  
 Blain, A. W., Chapman, S. C., Smail, I., & Ivison, R. 2004, ApJ, 611, 725  
 Brandt, W. N., Hornschemeier, A. E., Schneider, D. P., Alexander, D. M., Bauer, F. E., Garmire, G. P., & Vignali, C. 2001, ApJ, 558, L5  
 Bruzual, G. & Charlot, S. 2003, MNRAS, 344, 1000  
 Capak, P. et al. 2004, AJ, 127, 180  
 Chabrier, G. 2003, PASP, 115, 763  
 Chapman, S. C., Blain, A. W., Ivison, R. J., & Smail, I. R. 2003, Nature, 422, 695  
 Chapman, S. C., Blain, A. W., Smail, I., & Ivison, R. J. 2005, ApJ, 622, 772  
 Cohen, J. G. 2001, AJ, 121, 2895  
 Cohen, J. G., Cowie, L. L., Hogg, D. W., Songaila, A., Blandford, R., Hu, E. M., & Shopbell, P. 1996, ApJ, 471, L5+  
 Cohen, J. G., Hogg, D. W., Blandford, R., Cowie, L. L., Hu, E., Songaila, A., Shopbell, P., & Richberg, K. 2000, ApJ, 538, 29  
 Comastri, A. & Fiore, F. 2004, Ap&SS, 294, 63  
 Cowie, L. L., Barger, A. J., Hu, E. M., Capak, P., & Songaila, A. 2004, AJ, 127, 3137  
 Daddi, E. et al. 2004, ApJ, 600, L127  
 Dawson, S., Stern, D., Bunker, A. J., Spinrad, H., & Dey, A. 2001, AJ, 122, 598  
 Dickinson, M. 1998, in The Hubble Deep Field, ed. M. Livio, S. M. Fall, & P. Madau, 219–  
 Dickinson, M., Giavalisco, M., & The Goods Team. 2003a, in The Mass of Galaxies at Low and High Redshift, 324–  
 Dickinson, M., Papovich, C., Ferguson, H. C., & Budavári, T. 2003b, ApJ, 587, 25  
 Erb, D. K., Shapley, A. E., Pettini, M., Steidel, C. C., Reddy, N. A., & Adelberger, K. L. 2006a, ArXiv Astrophysics e-prints  
 Erb, D. K., Shapley, A. E., Steidel, C. C., Pettini, M., Adelberger, K. L., Hunt, M. P., Moorwood, A. F. M., & Cuby, J.-G. 2003, ApJ, 591, 101  
 Erb, D. K., Steidel, C. C., Shapley, A. E., Pettini, M., Reddy, N. A., & Adelberger, K. L. 2006b, ArXiv Astrophysics e-prints  
 —. 2006c, ArXiv Astrophysics e-prints  
 Fan, X. et al. 2001, AJ, 121, 54
- Forster Schreiber, N. M. et al. 2006, ArXiv Astrophysics e-prints  
 Franx, M. et al. 2003, ApJ, 587, L79  
 Giavalisco, M. et al. 2004, ApJ, 600, L93  
 Gilli, R. 2004, Advances in Space Research, 34, 2470  
 Hornschemeier, A. E. et al. 2001, ApJ, 554, 742  
 Hughes, D. H. et al. 1998, Nature, 394, 241  
 Hunt, M. P., Steidel, C. C., Adelberger, K. L., & Shapley, A. E. 2004, ApJ, 605, 625  
 Labb  , I. et al. 2005, astro-ph/0504219  
 Lowenthal, J. D. et al. 1997, ApJ, 481, 673  
 Madau, P., Ferguson, H. C., Dickinson, M. E., Giavalisco, M., Steidel, C. C., & Fruchter, A. 1996, MNRAS, 283, 1388  
 Nandra, K., Mushotzky, R. F., Arnaud, K., Steidel, C. C., Adelberger, K. L., Gardner, J. P., Teplitz, H. I., & Windhorst, R. A. 2002, ApJ, 576, 625  
 Oke, J. B., Cohen, J. G., Carr, M., Cromer, J., Dingizian, A., Harris, F. H., Labrecque, S., Lucinio, R., Schaaf, W., Epps, H., & Miller, J. 1995, PASP, 107, 375  
 Oke, J. B. & Gunn, J. E. 1983, ApJ, 266, 713  
 Papovich, C., Dickinson, M., & Ferguson, H. C. 2001, ApJ, 559, 620  
 Papovich, C. et al. 2006, ApJ, 640, 92  
 Pettini, M., Kellogg, M., Steidel, C. C., Dickins on, M., Adelberger, K. L., & Giavalisco, M. 1998, ApJ, 508, 539  
 Pettini, M., Shapley, A. E., Steidel, C. C., Cuby, J.-G., Dickinson, M., Moorwood, A. F. M., Adelberger, K. L., & Giavalisco, M. 2001, ApJ, 554, 981  
 Phillips, A. C., Guzman, R., Gallego, J., Koo, D. C., Lowenthal, J. D., Vogt, N. P., Faber, S. M., & Illingworth, G. D. 1997, ApJ, 489, 543  
 Pope, A., Borys, C., Scott, D., Conselice, C., Dickinson, M., & Mobasher, B. 2005, MNRAS, 358, 149  
 Reddy, N. A., Erb, D. K., Steidel, C. C., Shapley, A., Adelberger, K. L., & Pettini, M. 2005, ApJ, 633, 748  
 Reddy, N. A. & Steidel, C. C. 2004, ApJ, 603, L13  
 Reddy, N. A., Steidel, C. C., Fadda, D., Yan, L., Pettini, M., Shapley, A. E., Erb, D. K., & Adelberger, K. L. 2006, ArXiv Astrophysics e-prints  
 Richards, E. A. 2000, ApJ, 533, 611  
 Rudnick, G. et al. 2006, ArXiv Astrophysics e-prints  
 Salpeter, E. E. 1955, ApJ, 121, 161  
 Sawicki, M. & Yee, H. K. C. 1998, AJ, 115, 1329  
 Schiminovich, D., Arnouts, S., Milliard, B., & GALEX Science Team. 2003, American Astronomical Society Meeting Abstracts, 203,  
 Schmidt, M., Schneider, D. P., & Gunn, J. E. 1995, AJ, 110, 68  
 Shapley, A. E., Erb, D. K., Pettini, M., Steidel, C. C., & Adelberger, K. L. 2004, ApJ, 612, 108  
 Shapley, A. E., Steidel, C. C., Adelberger, K. L., Dickinson, M., Giavalisco, M., & Pettini, M. 2001, ApJ, 562, 95  
 Shapley, A. E., Steidel, C. C., Erb, D. K., Reddy, N. A., Adelberger, K. L., Pettini, M., Barmby, P., & Huang, J. 2005, ApJ, 626, 698  
 Shapley, A. E., Steidel, C. C., Pettini, M., & Adelberger, K. L. 2003, ApJ, 588, 65  
 Shaver, P. A., Wall, J. V., Kellermann, K. I., Jackson, C. A., & Hawkins, M. R. S. 1996, Nature, 384, 439

- Smail, I., Ivison, R. J., & Blain, A. W. 1997, ApJ, 490, L5+  
 Steidel, C. C., Adelberger, K. L., Giavalisco, M., Dickinson, M., &  
     Pettini, M. 1999, ApJ, 519, 1  
 Steidel, C. C., Adelberger, K. L., Shapley, A. E., Pettini, M.,  
     Dickinson, M., & Giavalisco, M. 2003, ApJ, 592, 728  
 Steidel, C. C., Giavalisco, M., Dickinson, M., & Adelberger, K. L.  
     1996, AJ, 112, 352  
 Steidel, C. C. & Hamilton, D. 1993, AJ, 105, 2017  
 Steidel, C. C., Hunt, M. P., Shapley, A. E., Adelberger, K. L.,  
     Pettini, M., Dickinson, M., & Giavalisco, M. 2002, ApJ, 576, 653  
 Steidel, C. C., Pettini, M., & Hamilton, D. 1995, AJ, 110, 2519  
 Steidel, C. C., Shapley, A. E., Pettini, M., Adelberger, K. L., Erb,  
     D. K., Reddy, N. A., & Hunt, M. P. 2004, ApJ, 604, 534  
 van Dokkum, P. G. et al. 2006, ApJ, 638, L59  
 Vanzella, E. et al. 2005, A&A, 434, 53  
 Wang, W.-H., Cowie, L. L., & Barger, A. J. 2004, ApJ, 613, 655  
 Williams, R. E. et al. 2000, AJ, 120, 2735  
 Williams, R. E., Blacker, B., Dickinson, M., Dixon, W. V. D.,  
     Ferguson, H. C., Fruchter, A. S., Giavalisco, M., Gilliland, R. L.,  
     Heyer, I., Katsanis, R., Levay, Z., Lucas, R. A., McElroy, D. B.,  
     Petro, L., Postman, M., Adorf, H.-M., & Hook, R. 1996, AJ, 112,  
     1335  
 Wilson, J. C. et al. 2003, in Instrument Design and Performance  
     for Optical/Infrared Ground-based Telescopes. Edited by Iye,  
     Masanori; Moorwood, Alan F. M. Proceedings of the SPIE,  
     Volume 4841, pp. 451-458 (2003)., 451-458  
 Wirth, G. D. et al. 2004, AJ, 127, 3121

TABLE 1  
SAMPLE STATISTICS TO  $\mathcal{R} = 25.5$

Candidates	$N_{\text{cand}}^{\text{a}}$	$\rho_{\text{cand}}^{\text{b}}$ (arcmin $^{-2}$ )	$N_{\text{obs}}^{\text{c}}$	$N_{z>1}^{\text{d}}$	$f_{z>1}^{\text{e}}$	$N_{z>1.4}^{\text{f}}$	$\langle z \rangle^{\text{g}}$
BM	470	$3.13 \pm 0.14$	67	63	0.94	49	$1.72 \pm 0.34$
BX	890	$5.93 \pm 0.20$	205	170	0.83	163	$2.19 \pm 0.40$
C	55	$0.37 \pm 0.05$	26	26	0.97	26	$3.11 \pm 0.21$
D	59	$0.39 \pm 0.05$	23	23	0.98	23	$3.05 \pm 0.22$
MD	78	$0.52 \pm 0.06$	26	25	0.96	25	$2.96 \pm 0.30$
<b>Total</b>	1552	$10.35 \pm 0.26$	347	307	0.88	286	$2.25 \pm 0.57$

<sup>a</sup>Number of photometric candidates.

<sup>b</sup>Surface density of photometric candidates to  $\mathcal{R} = 25.5$ .

<sup>c</sup>Number of objects with secure spectroscopic identifications.

<sup>d</sup>Number of objects with secure redshifts  $z > 1$ .

<sup>e</sup>Fraction of spectroscopically observed objects with  $z > 1$ . The foreground ( $z < 1$ ) contamination rates of the C, D, and MD samples are very low (< 5%) and we assume the interloper fractions derived over all fields of the  $z \sim 3$  Lyman Break Galaxy survey (Steidel et al. 2003). For the BM and BX samples, we assume foreground contamination fractions derived from the GOODS-N field, which are similar to those derived in other fields of the  $z \sim 2$  survey (Steidel et al. 2004).

<sup>f</sup>Number of objects with  $z > 1.4$

<sup>g</sup>Mean and standard deviation of redshift distribution for objects with  $z > 1$ .

TABLE 2  
GOODS-N  $U_nG\mathcal{R}$  GALAXIES WITH SPECTROSCOPIC REDSHIFTS

Name	$\alpha$ (J2000.0)	$\delta$ (J2000.0)	$z_{\text{em}}^{\text{a}}$	$z_{\text{abs}}^{\text{b}}$	Type <sup>c</sup>	$\mathcal{R}^{\text{d}}$ (mag)	$G - \mathcal{R}$ (mag)	$U_n - G^{\text{e}}$ (mag)	$J^{\text{f}}$ (mag)	$K_s^{\text{f}}$ (mag)	$m_{3.6\mu\text{m}}$ (mag)	$m_{4.5\mu\text{m}}$ (mag)	$m_{5.8\mu\text{m}}$ (mag)	$m_{8.0\mu\text{m}}$ (mag)	$f_{24\mu\text{m}}$ ( $\mu\text{Jy}$ )	Notes <sup>g</sup>
BX1035	12:36:13.03	62:10:21.1	...	2.236	GAL	23.46	0.37	0.68	...	...	22.48	22.47	22.11	22.59	33.0	
BX1040	12:36:17.81	62:10:11.2	2.469	2.466	GAL	24.84	0.22	0.68	...	...	22.94	23.27	...	...	...	
BX1042	12:35:50.89	62:13:33.5	2.613	2.601	GAL	24.83	0.50	1.16	...	...	23.09	23.03	23.13	22.88	15.2	
BX1050	12:36:18.80	62:10:37.4	...	2.322	GAL	24.71	0.40	0.73	...	...	23.49	23.51	23.46	...	...	
BX1051	12:35:52.97	62:13:36.8	...	2.098	GAL	24.23	0.14	0.57	...	...	23.07	...	...	...	203.9	
BX1055	12:35:59.59	62:13:07.5	2.496	2.486	GAL	24.09	0.24	0.81	...	...	23.12	23.23	...	...	...	
BX1060	12:36:06.40	62:12:29.1	...	2.081	GAL	24.22	0.43	0.84	...	...	21.74	21.73	21.93	...	67.3	
BX1064	12:36:30.34	62:09:45.3	...	2.086	GAL	24.20	0.28	0.61	23.60	22.63	23.00	23.11	23.16	23.76	26.0	
BX1065	12:36:09.84	62:11:39.0	...	2.701	GAL	24.01	0.43	1.04	...	...	22.41	22.60	...	...	13.3	
BX1069	12:36:45.82	62:08:08.2	0.000	0.000	STAR	21.95	0.38	0.77	...	...	23.37	24.01	...	...	...	
BX1071	12:36:20.10	62:11:12.6	...	1.996	GAL	24.41	0.27	0.76	23.71	24.10	22.84	23.06	...	...	...	
BX1073	12:36:43.35	62:08:19.6	0.087	0.087	GAL	20.59	0.40	0.82	...	...	21.71	22.15	22.66	22.56	41.2	
BX1074	12:36:19.38	62:11:25.5	1.754	1.745	GAL	24.01	0.13	0.40	22.74	21.92	22.11	22.09	22.00	...	40.5	
BX1075	12:36:14.45	62:11:52.1	...	2.221	GAL	24.08	0.35	1.04	...	...	22.47	22.49	22.30	...	10.8	
BX1080	12:36:18.39	62:11:39.2	...	2.390	GAL	24.38	0.51	1.15	...	...	22.55	22.53	22.72	23.02	47.3	S03-D7
BX1081	12:36:15.19	62:12:07.6	...	1.801	GAL	24.23	0.23	0.60	...	...	22.25	22.33	22.66	22.79	48.3	
BX1084	12:36:13.57	62:12:21.5	...	2.437	GAL	23.24	0.26	0.72	...	...	22.29	22.33	22.19	22.63	54.3	
BX1085	12:36:13.33	62:12:16.3	...	2.236	GAL	24.50	0.33	0.87	...	...	23.38	23.52	23.47	...	...	
BX1086	12:36:13.42	62:12:18.8	2.444	2.444	GAL	24.64	0.41	1.09	...	...	23.25	23.24	...	...	z from H $\alpha$	
BX1089	12:36:00.64	62:13:59.4	...	2.049	GAL	24.23	0.16	0.83	...	...	21.92	21.95	21.94	21.83	76.7	
BX1100	12:36:39.65	62:09:48.4	...	2.079	GAL	23.20	0.17	0.61	22.85	22.11	22.22	22.26	22.19	...	84.4	
BX1104	12:36:18.35	62:12:22.2	2.445	2.438	GAL	24.03	0.18	0.78	...	...	23.03	23.08	23.26	23.12	24.5	
BX1106	12:36:27.56	62:11:29.8	...	2.917	GAL	24.61	0.65	1.52	> 25.0	24.05	23.07	23.16	22.88	22.93	8.5	S03-oMD28
BX1112	12:36:15.65	62:13:05.3	0.170	...	GAL	24.26	0.21	0.87	...	...	24.18	24.77	...	...	...	
BX1116	12:36:09.05	62:13:59.1	...	2.048	GAL	24.10	0.13	0.62	...	...	22.59	22.66	22.50	23.06	18.4	
BX1120	12:36:07.62	62:14:16.6	0.169	...	GAL	24.64	0.43	1.31	...	...	24.95	...	...	...	...	
BX1121	12:36:13.24	62:13:39.6	1.878	1.878	GAL	23.80	0.13	0.46	...	...	21.77	21.78	22.07	22.22	55.5	
BX1125	12:36:25.00	62:12:23.6	2.222	...	GAL	25.20	0.18	0.94	> 25.0	> 24.4	24.00	24.37	...	...	...	
BX1126	12:36:11.91	62:13:58.7	...	1.942	GAL	24.59	0.07	0.32	...	...	23.61	23.74	...	...	...	
BX1129	12:36:56.94	62:08:48.7	...	1.973	GAL	22.80	0.21	0.58	...	...	21.52	21.60	21.46	22.00	104.4	
BX1130	12:36:33.17	62:11:34.1	0.080	...	GAL	20.65	0.30	0.84	20.50	20.20	21.05	20.99	21.15	21.57	152.8	B03-173
BX1132	12:36:03.91	62:15:08.3	...	2.112	GAL	24.41	0.45	0.98	...	...	22.72	22.64	22.53	...	...	
BX1140	12:36:08.51	62:14:48.0	1.487	...	GAL	24.69	0.10	0.36	...	...	22.62	22.74	22.71	...	9.1	
BX1145	12:36:10.12	62:14:49.2	...	2.325	GAL	25.40	0.17	0.51	...	...	24.13	24.23	...	...	...	
BX1157	12:36:18.30	62:14:09.1	2.083	2.078	GAL	24.14	0.14	0.34	...	...	21.99	22.00	21.62	21.84	...	
BX1161	12:36:59.39	62:09:21.9	...	1.891	GAL	23.71	0.37	0.59	...	...	21.85	21.87	22.24	22.47	23.3	
BX1164	12:36:24.20	62:13:32.6	2.598	2.588	GAL	24.49	0.22	0.85	> 25.0	> 24.4	24.05	24.43	...	...	...	
BX1166	12:36:20.32	62:14:04.9	1.334	...	GAL	24.54	0.09	0.30	22.95	23.13	23.28	23.55	...	...	12.5	
BX1169	12:36:28.27	62:13:15.3	...	1.871	GAL	23.82	0.14	0.43	23.04	22.30	22.47	22.45	22.54	23.14	40.7	
BX1170	12:36:31.94	62:12:51.8	2.445	2.441	GAL	24.26	0.35	1.04	23.23	22.58	22.38	22.49	22.06	...	32.9	
BX1172	12:36:54.35	62:10:18.3	2.811	2.802	GAL	24.50	0.55	1.19	> 25.0	> 24.4	24.05	24.31	...	...	S03-D2	
BX1174	12:36:47.82	62:11:06.1	2.349	...	GAL	24.37	0.19	0.49	24.40	23.72	23.07	23.36	...	...		
BX1178	12:36:33.52	62:12:51.8	0.000	0.000	STAR	23.23	0.01	0.42	23.38	22.64	24.01	...	...	...		
BX1183	12:37:08.51	62:08:54.7	2.043	2.039	GAL	24.67	0.37	1.00	...	...	23.25	23.51	...	...		
BX1185	12:36:12.60	62:15:30.0	2.207	2.203	GAL	24.99	0.47	0.96	...	...	22.54	22.46	22.41	22.52	44.1	
BX1186	12:36:13.20	62:15:26.2	...	2.079	GAL	25.02	0.22	0.53	...	...	24.66	24.53	...	...	...	
BX1192	12:36:16.83	62:15:14.3	...	1.996	GAL	24.22	0.15	0.86	...	...	21.52	21.56	21.47	21.67	111.6	
BX1197	12:36:18.89	62:15:06.8	2.599	2.587	GAL	24.13	0.17	0.80	> 25.0	> 24.4	22.73	22.76	...	...	31.9	
BX1201	12:36:14.13	62:15:41.8	...	2.000	GAL	24.00	0.18	0.71	...	...	22.94	22.99	23.04	...	29.0	
BX1204	12:36:21.73	62:14:52.6	2.209	2.200	GAL	24.27	0.32	1.13	23.27	22.38	22.51	22.62	22.76	23.21	15.8	
BX1208	12:36:41.67	62:12:38.7	2.589	...	GAL	24.44	0.30	0.79	23.66	23.99	23.76	24.17	...	...		
BX1209	12:36:37.07	62:13:11.8	0.348	...	GAL	24.63	0.30	0.88	> 25.0	23.07	23.96	23.93	...	...	13.1	
BX1214	12:36:44.65	62:12:27.2	...	1.879	GAL	23.99	0.23	0.60	22.67	22.10	22.05	21.96	21.97	22.39	46.9	
BX1217	12:37:08.47	62:09:47.1	...	2.170	GAL	24.73	0.27	0.89	23.40	22.82	23.23	23.24	23.27	23.44	...	

TABLE 2 — *Continued*

Name	$\alpha$ (J2000.0)	$\delta$ (J2000.0)	$z_{\text{em}}^{\text{a}}$	$z_{\text{abs}}^{\text{b}}$	Type <sup>c</sup>	$\mathcal{R}^{\text{d}}$ (mag)	$G - \mathcal{R}$ (mag)	$U_{\text{n}} - G^{\text{e}}$ (mag)	$J^{\text{f}}$ (mag)	$K_s^{\text{f}}$ (mag)	$m_{3.6\mu\text{m}}$ (mag)	$m_{4.5\mu\text{m}}$ (mag)	$m_{5.8\mu\text{m}}$ (mag)	$m_{8.0\mu\text{m}}$ (mag)	$f_{24\mu\text{m}}$ ( $\mu\text{Jy}$ )	Notes <sup>g</sup>
BX1218	12:36:41.69	62:12:58.0	...	:2.054	GAL	23.88	0.11	0.35	23.23	22.50	22.40	22.67	22.97	26.2		
BX1220	12:36:30.85	62:14:18.2	0.136	0.136	GAL	24.86	0.41	0.81	23.51	22.45	21.92	21.91	21.99	22.56	...	
BX1222	12:37:02.99	62:10:34.1	2.446	2.438	GAL	24.53	0.26	0.75	> 25.0	24.14	24.43	24.41	...	...	S03-MD18	
BX1223	12:36:18.22	62:15:51.6	:1.865	...	GAL	25.07	0.25	0.48	23.55	21.81	21.17	20.92	20.51	20.79	307.4 DRG	
BX1228	12:36:20.19	62:15:40.6	1.999	1.995	GAL	24.03	0.39	0.65	23.12	23.33	22.94	23.10	23.05	...	14.7	
BX1229	12:36:33.23	62:14:11.0	1.343	1.343	GAL	23.80	0.12	0.36	23.06	22.57	22.42	22.40	22.31	22.34	48.4	
BX1233	12:36:36.76	62:13:51.3	2.856	...	GAL	24.67	0.37	0.86	> 25.0	23.37	22.75	22.61	22.20	...	...	
BX1238	12:36:54.39	62:11:55.4	...	2.261	GAL	24.57	0.30	0.65	24.00	23.33	22.97	22.91	23.21	...	...	
BX1240	12:37:06.77	62:10:23.1	...	2.282	GAL	24.01	0.14	0.68	24.06	23.63	23.19	23.19	...	...		
BX1243	12:37:06.66	62:10:35.2	...	:2.037	GAL	23.99	0.27	0.52	23.21	22.99	22.68	22.71	22.67	...	...	
BX1244	12:37:02.55	62:11:05.0	...	1.012	GAL	23.68	0.07	0.27	> 25.0	> 24.4	22.35	22.48	22.70	...	35.7	
BX1245	12:36:16.28	62:16:30.4	2.097	2.089	GAL	23.82	-0.05	0.34	...	...	22.91	22.91	...	...	18.8	
BX1250	12:36:32.11	62:14:50.9	1.856	1.853	GAL	24.68	0.04	0.40	24.06	23.39	22.86	22.86	22.95	...	...	
BX1252	12:37:07.71	62:10:37.6	...	2.931	GAL	24.12	0.60	1.57	24.56	23.72	23.53	...	...	...		
BX1253	12:36:23.62	62:15:55.9	...	1.933	GAL	24.51	0.18	0.38	> 25.0	> 24.4	22.49	22.53	23.13	23.18	...	
BX1260	12:37:13.31	62:10:14.9	...	:1.714	GAL	24.98	0.50	1.02	22.97	21.60	21.51	21.45	21.83	105.7		
BX1264	12:37:09.38	62:10:46.3	2.942	...	GAL	24.76	0.14	0.80	> 25.0	23.75	...	...	...	...	S03-oMD24	
BX1265	12:36:33.35	62:15:04.4	2.437	2.431	GAL	23.93	0.17	1.02	24.27	22.74	23.20	23.27	23.42	23.33	...	
BX1267	12:36:22.67	62:16:21.6	1.996	1.996	GAL	23.90	0.13	0.51	22.84	22.17	23.45	...	...	48.7		
BX1269	12:37:10.37	62:10:49.2	...	2.275	GAL	23.53	0.45	1.00	22.97	21.96	21.85	21.78	21.77	22.15	89.1	
BX1270	12:36:51.42	62:13:00.6	0.089	0.089	GAL	22.93	0.28	0.95	22.81	22.89	23.97	24.35	...	...		
BX1274	12:37:11.35	62:10:44.2	2.599	2.594	GAL	24.29	0.25	0.93	24.02	23.87	22.80	23.02	...	...	26.6	
BX1277	12:37:18.60	62:09:55.5	...	2.268	GAL	23.87	0.14	0.61	22.89	23.08	23.11	23.28	...	...	27.0	
BX1279	12:36:19.45	62:17:01.1	0.995	...	GAL	24.79	-0.19	0.19	> 25.0	> 24.4	23.79	24.15	...	...	40.7	
BX1281	12:37:03.39	62:11:53.5	...	2.410	GAL	25.16	0.32	0.70	> 25.0	23.89	23.84	24.11	...	...	13.4 S03-D8	
BX1283	12:37:16.29	62:10:23.3	...	2.427	GAL	24.59	0.24	0.60	23.46	22.72	22.69	22.69	23.31	23.18	...	
BX1284	12:36:44.08	62:14:09.9	2.276	2.270	GAL	24.37	0.01	0.61	23.77	22.97	23.28	23.33	23.10	...	...	
BX1287	12:36:20.64	62:16:57.9	...	1.675	GAL	23.05	0.05	0.34	22.17	22.58	22.60	22.50	22.68	23.27	35.1	
BX1288	12:37:11.14	62:11:04.5	2.301	...	GAL	24.16	0.10	0.58	23.29	23.50	23.15	23.31	23.57	...	...	
BX1289	12:36:33.67	62:15:32.9	...	2.488	GAL	24.15	0.34	1.16	23.47	22.64	22.76	22.77	22.90	22.91	18.8	
BX1290	12:36:35.55	62:15:21.8	2.980	...	GAL	24.69	0.39	0.79	> 25.0	> 24.4	23.81	24.16	...	...	S03-oMD54	
BX1291	12:37:00.11	62:12:25.2	...	2.052	GAL	23.56	0.30	0.80	23.49	23.17	23.05	23.15	23.19	23.71	22.4	
BX1293	12:36:46.52	62:14:07.5	0.128	...	GAL	24.22	0.33	0.67	23.53	23.43	21.07	21.09	21.06	20.79	199.2	
BX1296	12:36:20.91	62:17:09.5	1.989	1.988	GAL	24.15	0.26	0.59	22.82	21.75	21.19	20.96	20.67	21.00	263.7	
BX1297	12:37:13.08	62:11:02.2	...	2.274	GAL	24.53	0.35	0.82	23.25	22.00	21.89	21.85	21.76	22.19	...	
BX1299	12:36:53.24	62:13:22.2	1.654	1.649	GAL	23.49	0.36	0.61	23.38	22.32	22.94	22.96	23.49	...	18.7	
BX1300	12:36:54.76	62:13:14.7	2.288	2.288	GAL	24.55	0.21	0.65	24.08	23.34	22.93	23.06	...	...		
BX1303	12:37:11.20	62:11:18.7	2.305	2.304	GAL	24.72	0.11	0.81	24.24	22.85	23.55	23.35	...	...	15.1 DRG	
BX1305	12:36:50.12	62:14:01.0	2.238	2.231	GAL	24.77	0.14	0.72	23.35	23.00	22.80	22.76	22.68	22.76	73.1	
BX1307	12:36:48.33	62:14:16.7	...	2.002	GAL	23.30	0.20	0.74	22.69	21.83	21.69	21.61	21.34	21.44	145.5	
BX1311	12:36:30.54	62:16:26.1	2.490	2.479	GAL	23.29	0.21	0.81	22.94	22.30	22.65	22.74	22.60	...	24.0	
BX1312	12:37:02.27	62:12:43.2	0.107	0.107	GAL	22.72	0.46	1.04	22.32	22.71	23.86	...	...	45.4		
BX1313	12:37:04.04	62:12:33.8	2.637	2.632	GAL	24.31	0.42	0.99	> 25.0	> 24.4	23.68	23.71	...	...		
BX1315	12:36:30.10	62:16:35.9	...	1.671	GAL	23.77	0.19	0.41	22.62	22.06	21.79	21.75	21.91	22.05	64.8	
BX1316	12:37:20.70	62:10:40.7	2.088	...	GAL	24.26	0.20	0.55	23.16	22.41	22.04	21.99	21.79	...	...	
BX1317	12:36:25.36	62:17:08.0	1.792	1.787	GAL	23.28	0.16	0.41	22.44	21.78	22.26	22.25	22.32	22.50	53.9	
BX1319	12:37:04.26	62:12:39.5	1.109	1.109	GAL	23.33	0.31	0.62	22.54	21.82	21.34	21.23	21.17	21.46	102.1	
BX1321	12:36:48.31	62:14:26.5	0.139	...	—	19.22	0.32	0.91	18.72	18.46	19.37	19.74	19.73	17.68	434.8 B03-251	
BX1322	12:37:06.54	62:12:24.9	2.449	2.438	GAL	23.72	0.31	0.57	24.01	22.77	23.25	23.28	...	...	31.9	
BX1324	12:37:12.95	62:11:44.5	1.821	1.815	GAL	24.38	0.46	1.03	22.85	22.15	21.79	21.70	21.90	22.09	143.0	
BX1326	12:36:35.71	62:16:14.9	2.984	...	GAL	24.49	0.40	0.73	> 25.0	23.90	23.81	24.17	...	...		
BX1327	12:36:57.51	62:13:44.2	2.209	...	GAL	24.05	0.21	0.44	23.13	22.51	22.92	23.00	22.98	23.45	23.3	
BX1329	12:36:54.62	62:14:07.7	...	:1.987	GAL	24.69	-0.04	0.45	23.95	23.79	24.46	...	...	8.2		
BX1330	12:36:48.91	62:14:50.9	...	2.363	GAL	23.73	0.05	0.61	23.66	22.72	22.91	22.95	22.86	...	24.8	
BX1332	12:37:17.13	62:11:39.9	2.218	2.209	GAL	23.64	0.32	0.92	23.35	22.50	22.53	22.41	...	29.7		

Reddy et al.

TABLE 2 — *Continued*

Name	$\alpha$ (J2000.0)	$\delta$ (J2000.0)	$z_{\text{em}}^{\text{a}}$	$z_{\text{abs}}^{\text{b}}$	Type <sup>c</sup>	$\mathcal{R}^{\text{d}}$ (mag)	$G - \mathcal{R}$ (mag)	$U_n - G^{\text{e}}$ (mag)	$J^{\text{f}}$ (mag)	$K_s^{\text{f}}$ (mag)	$m_{3.6\mu\text{m}}$ (mag)	$m_{4.5\mu\text{m}}$ (mag)	$m_{5.8\mu\text{m}}$ (mag)	$m_{8.0\mu\text{m}}$ (mag)	$f_{24\mu\text{m}}$ ( $\mu\text{Jy}$ )	Notes <sup>g</sup>
BX1334	12:36:46.64	62:15:17.0	3.371	...	GAL	25.11	0.46	1.19	> 25.0	23.22	...	...	...	...	...	S03-M28; DRG
BX1335	12:36:44.69	62:15:31.2	...	:2.453	AGN?	25.15	0.28	0.94	23.74	22.84	22.90	22.89	22.67	22.88	19.3	
BX1339	12:36:25.09	62:17:56.8	1.993	1.984	GAL	24.60	-0.05	0.48	...	...	23.06	23.03	22.63	...	...	
BX1343	12:37:08.77	62:12:57.8	...	2.268	GAL	23.98	0.17	0.82	22.88	22.57	22.45	22.51	22.45	...	21.0	
BX1348	12:37:05.84	62:13:29.3	1.923	1.919	GAL	24.76	0.05	0.29	23.84	23.89	23.88	...	...	...	24.8	
BX1349	12:36:57.27	62:14:29.7	...	1.873	GAL	24.29	0.41	0.74	22.93	22.18	21.61	21.45	21.49	21.68	104.8	
BX1350	12:37:05.50	62:13:34.6	...	:2.830	GAL	24.56	0.45	1.14	> 25.0	> 24.4	...	...	...	...	...	S03-MD37
BX1351	12:36:59.40	62:14:04.7	0.089	0.089	GAL	20.17	0.45	1.01	19.69	19.83	21.53	21.90	21.98	21.55	...	
BX1353	12:36:31.15	62:17:39.9	...	2.505	GAL	24.28	0.24	0.61	22.92	22.03	21.82	21.75	21.92	22.14	65.7	
BX1354	12:37:17.25	62:12:20.3	2.088	2.088	GAL	24.98	-0.10	0.38	> 25.0	> 24.4	24.50	...	...	...	...	
BX1355	12:36:43.16	62:16:20.1	...	2.307	GAL	24.09	0.13	1.07	23.77	22.98	22.34	22.53	22.94	...	...	
BX1358	12:36:59.46	62:14:27.7	2.943	...	GAL	24.83	0.49	1.45	> 25.0	23.73	24.11	24.25	...	...	...	
BX1361	12:36:30.47	62:17:53.9	...	:1.849	GAL	25.48	-0.04	0.22	> 25.0	23.43	24.22	...	...	...	DRG	
BX1362	12:36:42.57	62:16:29.4	...	1.664	GAL	24.55	0.05	0.28	23.56	22.83	22.08	22.34	...	...		
BX1363	12:37:27.40	62:11:12.7	...	2.297	GAL	23.82	0.33	0.76	22.89	22.15	22.58	22.59	22.52	22.76	58.8	
BX1364	12:37:23.74	62:11:41.2	...	2.183	GAL	24.27	0.22	0.74	23.56	22.82	22.65	22.64	22.78	23.14	11.5	
BX1368	12:36:48.24	62:15:56.2	2.446	2.440	GAL	23.79	0.30	0.96	23.34	22.45	22.35	22.60	22.43	22.40	71.0	
BX1371	12:37:16.57	62:12:45.2	0.947	...	GAL	24.23	0.30	0.95	23.84	23.79	24.49	24.95	...	...	...	
BX1374	12:36:57.90	62:15:07.0	0.116	0.116	GAL	23.80	0.26	0.88	23.27	23.41	24.13	...	...	...		
BX1376	12:36:52.96	62:15:45.5	2.434	2.426	GAL	24.48	0.01	0.70	24.05	23.95	23.93	24.05	...	...	...	
BX1378	12:37:02.02	62:14:43.4	...	1.971	GAL	23.90	0.33	0.66	23.14	22.75	22.42	22.40	22.43	23.15	29.4	
BX1387	12:36:56.32	62:15:52.4	...	2.324	GAL	24.77	0.17	0.61	23.72	23.89	23.61	23.60	23.40	...	15.2	
BX1388	12:36:44.84	62:17:15.8	...	2.032	GAL	24.55	0.27	0.99	22.63	21.77	21.55	21.43	21.23	21.54	151.7	
BX1391	12:37:13.87	62:13:54.9	...	1.906	GAL	24.06	0.35	0.57	23.14	22.98	22.46	22.45	22.52	23.19	...	
BX1392	12:37:25.92	62:12:06.4	0.089	...	GAL	21.58	0.37	0.94	21.27	21.23	22.48	22.85	23.35	23.04	...	
BX1397	12:37:04.12	62:15:09.8	...	2.133	GAL	24.12	0.14	0.76	22.85	22.69	22.47	22.36	22.30	22.50	30.2	
BX1399	12:37:18.30	62:13:32.6	...	2.033	GAL	25.22	0.23	0.73	23.91	23.49	22.73	22.84	22.51	...	20.9	
BX1400	12:37:06.09	62:15:01.5	:3.239	...	GAL	23.77	0.52	1.21	23.17	23.41	23.79	24.10	...	...	...	
BX1401	12:37:02.93	62:15:22.5	...	2.481	GAL	23.47	0.41	0.87	22.38	21.73	21.76	21.57	21.35	21.60	41.2	
BX1403	12:37:25.12	62:12:49.5	...	:1.706	GAL	24.63	0.32	0.52	> 25.0	> 24.4	22.85	22.82	...	...	15.4	
BX1408	12:36:57.40	62:16:18.2	...	2.482	GAL	24.83	0.64	1.47	24.13	22.68	22.49	22.38	22.28	22.63	31.4	S03-MD40; DRG
BX1409	12:36:47.41	62:17:28.7	...	2.237	GAL	24.66	0.49	1.17	23.28	21.89	22.23	22.22	22.10	22.34	52.1	DRG
BX1420	12:36:50.87	62:17:12.4	...	2.133	GAL	23.79	0.45	1.01	22.84	22.34	22.06	22.13	...	...	18.5	
BX1425	12:37:17.96	62:14:17.6	...	1.864	GAL	24.65	0.02	0.28	23.44	23.66	23.30	23.28	23.50	...	...	
BX1427	12:37:33.28	62:12:33.8	...	2.548	GAL	24.54	0.39	0.85	...	...	22.98	22.97	22.82	...	8.3	
BX1431	12:36:58.48	62:16:45.5	2.006	1.996	GAL	24.00	0.09	0.45	> 25.0	23.13	23.11	23.25	...	...	DRG	
BX1434	12:37:16.80	62:14:38.8	...	1.994	GAL	24.49	0.26	0.51	23.62	23.21	23.14	23.18	...	...	...	
BX1439	12:36:53.66	62:17:24.3	2.191	2.186	GAL	23.90	0.26	0.79	22.78	21.54	21.91	21.82	21.82	20.93	85.3	
BX1443	12:36:44.87	62:18:37.9	...	1.684	GAL	23.33	0.31	0.57	...	...	20.85	20.67	20.81	20.93	194.0	
BX1446	12:36:43.42	62:18:55.3	2.326	2.315	GAL	24.21	0.16	0.71	...	...	23.08	23.00	...	...	...	
BX1451	12:37:13.22	62:15:31.7	...	2.245	GAL	24.58	0.40	0.86	23.54	22.84	22.37	22.23	22.36	22.47	36.0	
BX1458	12:37:26.95	62:14:03.6	...	1.864	GAL	24.84	0.35	0.68	23.19	23.05	22.63	22.78	...	...	52.4	
BX1460	12:36:56.80	62:17:25.5	3.137	3.131	GAL	24.70	0.41	1.30	24.39	23.68	23.30	23.72	23.18	...	...	
BX1461	12:36:49.54	62:18:33.2	2.107	2.107	GAL	24.77	0.23	0.63	...	...	23.54	23.48	...	23.77	...	
BX1476	12:37:19.55	62:15:20.8	1.930	1.927	GAL	25.19	0.15	0.37	> 25.0	> 24.4	22.46	23.04	...	...	...	
BX1479	12:37:15.42	62:16:03.9	2.383	2.371	GAL	24.39	0.16	0.79	23.77	23.12	23.03	23.08	22.68	...	10.9	
BX1480	12:37:25.43	62:14:56.2	...	2.545	GAL	24.28	0.53	1.13	24.06	23.32	22.65	22.54	22.52	22.80	18.3	
BX1485	12:37:28.12	62:14:39.9	...	2.548	GAL	23.29	0.35	0.96	22.96	22.02	21.36	21.32	21.19	21.30	315.9	
BX1495	12:37:24.88	62:15:22.4	2.251	2.244	GAL	24.98	0.20	0.73	> 25.0	23.32	23.48	23.40	...	...	...	DRG
BX1501	12:37:41.58	62:13:22.2	1.879	1.875	GAL	23.78	0.16	0.46	...	...	22.19	22.16	22.28	22.74	43.3	
BX1504	12:37:41.90	62:13:33.7	2.869	2.858	GAL	24.34	0.52	1.42	...	...	23.75	23.71	23.55	...	...	
BX1505	12:36:59.12	62:18:35.8	1.012	...	GAL	24.49	0.11	0.34	...	...	22.93	22.94	22.57	22.00	256.2	
BX1510	12:37:27.13	62:15:28.3	...	:2.072	GAL	24.90	0.15	0.57	23.54	23.98	23.52	23.50	...	...	...	
BX1514	12:37:14.93	62:16:59.8	...	2.135	GAL	24.90	0.29	0.56	23.48	> 24.4	22.68	22.51	22.96	22.80	22.2	
BX1525	12:37:24.15	62:16:11.6	1.689	1.689	GAL	24.15	0.28	0.56	22.44	21.56	21.59	21.41	21.55	21.60	120.4	

Spectroscopic Survey of GOODES-North

TABLE 2 — *Continued*

Name	$\alpha$ (J2000.0)	$\delta$ (J2000.0)	$z_{\text{em}}^{\text{a}}$	$z_{\text{abs}}^{\text{b}}$	Type <sup>c</sup>	$\mathcal{R}^{\text{d}}$ (mag)	$G - \mathcal{R}$ (mag)	$U_{\text{n}} - G^{\text{e}}$ (mag)	$J^{\text{f}}$ (mag)	$K_s^{\text{f}}$ (mag)	$m_{3.6\mu\text{m}}$ (mag)	$m_{4.5\mu\text{m}}$ (mag)	$m_{5.8\mu\text{m}}$ (mag)	$m_{8.0\mu\text{m}}$ (mag)	$f_{24\mu\text{m}}$ ( $\mu\text{Jy}$ )	Notes <sup>g</sup>
BX1529	12:37:01.68	62:18:48.6	0.232	...	GAL	24.31	0.27	0.51	...	...	...	...	...	...	...	...
BX1530	12:37:22.85	62:16:27.6	...	2.421	GAL	24.40	0.25	0.84	24.18	23.19	23.41	23.33	...	22.83	...	
BX1535	12:37:07.18	62:18:30.1	...	2.299	GAL	24.31	0.33	0.97	...	...	23.18	23.17	23.27	23.46	...	
BX1542	12:36:55.06	62:20:05.2	1.018	...	GAL	24.72	0.11	0.31	...	...	23.34	23.70	...	...	...	
BX1544	12:37:14.85	62:17:47.3	...	2.486	GAL	24.27	0.24	1.13	...	...	...	...	...	...	...	
BX1548	12:37:00.49	62:19:30.3	0.223	...	GAL	23.79	0.46	0.89	...	...	23.95	24.71	...	...	...	
BX1557	12:37:27.17	62:16:31.7	...	1.776	GAL	23.74	0.31	0.80	22.99	23.00	21.64	21.73	21.29	22.85	167.9	
BX1559	12:37:29.41	62:15:40.1	...	2.408	GAL	24.19	0.07	0.59	23.84	23.53	23.10	23.08	...	...	85.8	
BX1564	12:37:23.47	62:17:20.0	...	2.218	GAL	23.28	0.27	1.01	22.21	21.44	21.77	21.69	21.57	21.98	74.8	
BX1567	12:37:23.17	62:17:23.9	...	2.225	GAL	23.50	0.18	1.05	22.31	22.00	21.96	21.86	21.79	22.03	34.1	
BX1568	12:36:54.06	62:20:48.1	...	1.787	GAL	23.46	0.08	0.44	...	...	22.68	22.63	22.68	23.30	25.5	
BX1572	12:36:58.51	62:20:29.3	...	1.782	GAL	24.32	0.25	0.59	...	...	23.43	23.47	23.63	...	...	
BX1574	12:37:25.95	62:17:10.1	...	1.808	GAL	24.24	0.22	0.66	22.66	22.33	22.00	21.90	22.08	22.12	55.3	
BX1579	12:37:38.93	62:15:41.0	0.190	...	GAL	22.98	0.38	0.62	...	...	23.65	24.17	...	...	58.1	
BX1586	12:37:24.91	62:17:40.8	...	1.901	GAL	24.44	0.41	0.82	23.54	23.10	23.02	23.02	...	...	22.5	
BX1588	12:37:02.54	62:20:20.9	...	2.221	GAL	23.22	0.30	1.17	> 25.0	> 24.4	21.58	21.48	21.24	21.52	129.7	
BX1591	12:37:28.21	62:17:22.6	2.050	2.048	GAL	24.45	0.21	0.52	23.03	22.97	23.17	23.24	23.49	...	10.0	
BX1605	12:37:21.51	62:18:30.6	1.977	1.970	GAL	23.89	-0.07	0.19	...	...	23.29	23.36	...	...	...	
BX1616	12:37:32.75	62:17:27.6	...	2.205	GAL	25.29	0.13	0.35	...	...	23.79	...	...	...	...	
BX1617	12:37:04.16	62:20:50.8	2.323	2.317	GAL	25.15	0.15	0.68	...	...	23.96	23.99	...	23.37	...	
BX1630	12:37:25.95	62:18:32.5	2.222	2.217	GAL	24.35	0.03	0.52	...	...	23.40	23.49	...	23.54	...	
BX1636	12:37:20.03	62:19:23.1	2.306	2.295	GAL	24.08	0.44	1.16	...	...	21.93	21.82	21.66	21.82	71.2	
BX1637	12:37:04.82	62:21:11.5	2.487	...	AGN	24.92	-0.01	0.81	...	...	23.38	22.76	21.84	20.93	109.4	
BX1641	12:37:08.89	62:20:44.7	1.433	...	GAL	24.20	0.01	0.26	...	...	23.79	23.93	...	...	...	
BX1642	12:37:32.40	62:17:50.8	2.010	2.004	GAL	24.29	0.25	0.46	...	...	22.97	22.95	...	...	...	
BX1650	12:37:24.11	62:19:04.7	2.100	2.094	GAL	23.24	0.18	0.74	...	...	22.10	22.05	21.95	22.42	37.5	
BX1655	12:37:32.30	62:18:16.3	0.157	...	GAL	24.37	0.41	1.21	...	...	24.55	24.92	...	...	...	
BX1669	12:37:48.40	62:16:34.8	0.118	...	GAL	23.24	0.35	0.96	...	...	23.22	23.41	...	23.44	...	
BX1676	12:37:36.68	62:18:02.1	0.188	...	GAL	23.49	0.42	0.80	...	...	23.58	23.81	...	...	51.0	
BX1694	12:37:33.82	62:18:46.3	2.009	2.005	GAL	23.66	0.11	0.53	...	...	22.50	22.58	22.28	...	13.8	
BX1708	12:37:32.65	62:19:10.6	...	1.987	GAL	24.50	0.45	1.00	...	...	21.46	21.23	21.03	21.34	208.3	
BX1782	12:36:57.46	62:08:38.0	0.177	0.177	GAL	22.27	0.43	0.75	...	...	22.64	23.17	...	...	30.3	
BX1790	12:36:59.31	62:09:31.2	...	2.990	GAL	23.81	0.62	1.17	22.58	23.20	23.20	23.09	...	...	...	
BX1796	12:36:27.51	62:14:18.8	0.089	...	GAL	22.70	0.49	0.70	22.43	22.15	22.43	22.93	22.71	...	...	
BX1805	12:36:38.64	62:14:21.8	0.306	0.306	GAL	22.80	0.48	0.80	21.66	21.10	21.99	22.37	22.67	22.59	95.2	
BX1808	12:36:59.54	62:12:14.2	...	1.943	GAL	24.09	0.43	0.68	23.33	23.38	23.01	23.29	...	...	...	
BX1815	12:37:15.22	62:11:02.6	0.000	0.000	STAR	19.64	0.54	1.08	19.48	19.87	21.13	21.68	22.08	22.81	...	
BX1816	12:36:44.13	62:14:50.7	...	2.095	GAL	24.25	0.53	0.87	23.16	22.00	21.42	21.26	21.25	21.62	...	
BX1817	12:36:23.27	62:16:43.2	1.862	1.858	GAL	24.54	0.46	0.76	23.66	22.69	21.65	21.77	21.75	...	43.4	
BX1820	12:37:19.43	62:11:13.8	...	2.457	GAL	24.11	0.65	1.35	23.07	22.07	21.64	21.49	21.27	21.32	105.6	
BX1821	12:37:12.63	62:12:10.4	...	2.590	GAL	24.79	0.60	1.11	23.93	23.54	23.28	23.44	22.87	...	15.1	
BX1822	12:37:05.74	62:13:03.2	0.109	...	GAL	22.05	0.59	1.14	22.03	21.91	22.78	23.24	23.03	...	...	
BX1823	12:37:15.40	62:12:17.9	...	1.818	GAL	24.65	0.49	0.78	22.24	21.33	20.88	20.76	20.78	21.02	127.4	
BX1826	12:37:17.38	62:12:46.8	...	2.929	GAL	24.67	0.52	1.02	23.99	23.78	23.49	23.52	...	...	32.0	
BX1827	12:36:56.63	62:15:19.0	1.988	...	GAL	24.84	0.56	1.12	24.48	23.28	23.42	23.46	...	...	...	
BX1828	12:37:16.22	62:13:24.3	...	2.967	GAL	24.09	0.66	1.40	23.35	23.45	24.06	24.75	...	...	...	
BX1833	12:37:11.13	62:14:33.8	0.000	0.000	STAR	22.12	0.59	1.02	22.30	22.01	22.56	22.91	...	...	...	
BX1841	12:37:02.63	62:16:33.9	...	2.373	GAL	24.70	0.47	1.04	23.46	23.12	22.57	22.81	22.80	...	...	
BX1848	12:37:25.86	62:14:42.4	2.648	...	GAL	25.05	0.45	0.81	> 25.0	> 24.4	23.93	24.32	...	...	12.4	
BX1851	12:37:29.99	62:15:59.5	0.215	...	GAL	22.96	0.48	0.72	22.31	22.07	22.44	22.60	...	...	...	
BX1856	12:37:22.40	62:17:18.0	0.232	...	GAL	23.03	0.51	0.82	22.51	22.34	23.49	23.87	23.82	23.30	...	
BX1860	12:37:30.81	62:16:54.7	...	2.504	GAL	24.80	0.51	0.85	> 25.0	23.71	22.73	22.75	22.57	...	29.6	
BX28	12:37:17.78	62:09:37.8	0.229	...	GAL	23.74	0.61	0.78	23.54	23.11	...	...	22.71	22.45	...	
BX82	12:37:05.37	62:10:45.3	1.023	...	GAL	24.41	0.58	0.19	23.29	22.94	23.30	23.55	...	...	...	
BX84	12:37:13.74	62:10:42.0	2.166	2.161	GAL	24.15	0.22	0.80	> 25.0	> 24.4	22.08	21.98	21.88	22.30	79.0	

TABLE 2 — *Continued*

Name	$\alpha$ (J2000.0)	$\delta$ (J2000.0)	$z_{\text{em}}^{\text{a}}$	$z_{\text{abs}}^{\text{b}}$	Type <sup>c</sup>	$\mathcal{R}^{\text{d}}$ (mag)	$G - \mathcal{R}$ (mag)	$U_n - G^{\text{e}}$ (mag)	$J^{\text{f}}$ (mag)	$K_s^{\text{f}}$ (mag)	$m_{3.6\mu\text{m}}$ (mag)	$m_{4.5\mu\text{m}}$ (mag)	$m_{5.8\mu\text{m}}$ (mag)	$m_{8.0\mu\text{m}}$ (mag)	$f_{24\mu\text{m}}$ ( $\mu\text{Jy}$ )	Notes <sup>g</sup>
BX150	12:37:14.98	62:12:07.9	2.281	2.273	GAL	24.64	0.54	0.53	> 25.0	> 24.4	22.34	22.12	21.87	...	46.9	
BX160	12:37:20.07	62:12:23.0	2.462	2.458	AGN	24.02	0.74	0.92	22.83	21.87	21.52	21.32	20.98	20.95	142.2	
BX184	12:37:19.28	62:13:00.6	1.998	...	GAL	24.22	0.70	0.99	23.42	23.46	22.80	22.95	...	...	...	
BX274	12:36:53.60	62:15:25.0	0.000	0.000	STAR	18.57	0.33	0.96	18.48	18.96	20.07	20.58	21.05	21.76	...	
BX283	12:37:24.35	62:15:58.3	0.129	...	GAL	23.41	0.44	0.84	> 25.0	> 24.4	24.55	24.75	...	...	...	
BX289	12:37:00.47	62:16:04.9	0.941	...	GAL	24.49	0.69	0.22	23.39	23.25	23.35	23.87	...	...	106.6	
BX305	12:36:37.13	62:16:28.7	...	2.482	GAL	24.28	0.79	1.30	23.63	21.96	22.03	22.00	21.90	21.71	69.4	DRG
BX308	12:37:02.66	62:16:34.0	...	2.376	GAL	24.87	0.46	0.95	> 25.0	> 24.4	22.53	22.75	22.79	...	...	
BX313	12:36:29.66	62:16:45.1	...	2.323	GAL	24.34	0.42	0.60	> 25.0	> 24.4	22.65	22.58	22.36	22.55	48.8	
BX341	12:36:22.26	62:17:30.9	2.117	2.117	GAL	23.56	0.71	0.27	23.77	22.73	22.47	22.58	...	22.91	...	
BM1008	12:35:47.95	62:12:52.3	1.801	1.798	GAL	23.58	0.24	0.25	...	...	22.68	22.60	23.20	22.90	27.5	
BM1010	12:36:08.08	62:10:44.7	...	1.346	GAL	24.03	0.16	0.18	...	...	22.69	22.88	...	...	37.4	
BM1011	12:35:51.57	62:12:42.0	1.677	1.677	GAL	23.90	0.28	0.33	...	...	22.21	22.25	22.40	23.06	20.9	
BM1017	12:36:11.72	62:10:39.3	...	:2.371	GAL	24.58	0.17	0.20	...	...	22.99	22.91	...	...	20.6	
BM1030	12:35:55.26	62:14:01.2	1.143	1.142	GAL	24.29	0.20	0.37	...	...	22.23	22.34	22.25	...	24.5	
BM1048	12:36:11.63	62:13:18.3	1.381	1.379	GAL	23.50	0.23	0.23	...	...	22.10	22.22	22.47	22.65	21.7	
BM1053	12:36:18.48	62:12:45.9	1.460	1.457	GAL	24.99	0.09	-0.02	...	...	24.02	24.32	...	...	15.7	
BM1061	12:36:15.82	62:13:26.0	2.089	...	GAL	25.37	0.02	-0.05	...	...	23.77	23.96	...	...	...	
BM1063	12:36:21.37	62:12:52.9	...	2.087	GAL	24.46	0.20	0.39	23.14	22.84	22.53	22.54	22.46	...	36.9	
BM1064	12:36:32.06	62:11:40.0	...	1.524	GAL	23.57	0.18	0.28	22.54	22.55	22.48	22.57	23.00	...	25.2	
BM1069	12:36:11.63	62:14:16.5	...	2.028	GAL	24.43	0.27	0.36	...	...	21.72	21.67	21.56	22.05	91.1	
BM1072	12:36:04.15	62:15:21.0	1.143	...	GAL	23.48	0.10	0.29	...	...	22.36	22.69	23.32	...	...	
BM1074	12:36:28.77	62:12:39.4	0.880	...	GAL	24.32	0.11	0.00	23.63	23.42	23.33	23.99	23.26	...	72.0	
BM1083	12:36:06.67	62:15:50.7	2.414	...	QSO	23.34	0.25	0.26	...	...	21.59	21.34	20.73	20.47	112.9	B03-77
BM1092	12:36:13.42	62:15:17.7	1.479	...	GAL	24.07	0.12	0.31	...	...	22.84	22.86	23.03	23.54	...	
BM1095	12:36:24.64	62:14:18.6	1.450	1.445	GAL	24.31	-0.01	0.15	23.17	23.66	23.37	23.67	...	...	...	
BM1098	12:36:51.16	62:11:28.0	...	1.671	GAL	23.76	0.20	0.37	22.77	22.47	22.09	22.01	22.45	22.63	30.2	
BM1099	12:37:03.45	62:10:09.1	...	:1.662	GAL	24.67	0.23	0.35	23.73	23.16	23.08	23.15	...	...	21.1	
BM1119	12:37:03.70	62:11:22.6	...	1.717	GAL	23.29	0.28	0.32	22.30	21.74	21.60	21.50	21.32	21.56	152.6	B03-327
BM1121	12:36:58.38	62:12:13.9	1.020	1.020	GAL	23.11	0.26	0.22	22.52	22.15	22.46	...	...	...	21.5	
BM1122	12:37:02.62	62:11:56.7	1.994	1.986	GAL	23.96	0.17	0.33	24.18	24.00	23.27	23.30	...	...	...	
BM1132	12:36:53.07	62:13:44.3	...	:1.901	GAL	23.76	0.26	0.40	23.13	22.63	22.98	23.06	23.08	23.27	...	
BM1135	12:36:49.76	62:14:14.9	...	1.872	GAL	23.57	0.29	0.43	22.44	21.76	21.63	21.57	21.49	21.96	111.4	
BM1136	12:36:52.75	62:13:54.8	1.355	...	GAL	22.15	0.16	0.23	21.53	21.36	21.15	21.11	21.37	21.16	99.5	B03-272
BM1139	12:37:22.12	62:10:46.6	1.919	...	GAL	24.10	0.25	0.18	24.37	23.17	22.46	22.61	...	...	220.8	
BM1144	12:36:43.72	62:15:46.2	...	:1.660	GAL	25.09	0.22	0.40	23.47	22.92	22.73	22.70	22.91	...	...	
BM1146	12:37:10.65	62:12:56.2	...	:1.926	GAL	24.30	0.09	0.06	23.88	23.29	23.20	23.55	...	...	...	
BM1148	12:36:46.15	62:15:51.1	2.053	2.045	GAL	23.38	0.20	0.29	24.43	23.08	23.11	23.24	...	23.08	14.5	
BM1149	12:36:34.79	62:17:10.1	1.631	1.629	GAL	24.58	0.02	0.16	> 25.0	> 24.4	24.15	...	...	...	...	
BM1153	12:36:48.46	62:15:59.5	2.450	2.439	GAL	24.64	0.32	0.47	23.83	22.85	21.65	21.43	21.42	21.54	123.0	
BM1155	12:37:23.98	62:12:12.1	2.024	2.015	GAL	23.99	0.08	0.15	23.25	23.50	23.21	23.28	...	...	...	
BM1156	12:37:04.34	62:14:46.3	2.211	...	AGN	24.62	-0.01	-0.21	22.94	22.15	22.10	21.94	21.18	19.97	324.4	S03-oMD49
BM1158	12:37:18.58	62:13:15.0	...	1.521	GAL	23.35	0.28	0.48	22.19	21.94	21.75	21.72	21.96	21.67	64.8	
BM1159	12:37:13.32	62:13:56.4	...	1.016	GAL	22.87	0.10	0.08	22.13	22.03	21.97	22.41	22.79	22.62	22.1	
BM1160	12:36:55.63	62:16:01.9	1.364	...	GAL	24.36	0.28	0.36	23.43	23.41	22.93	23.01	23.70	...	19.8	
BM1161	12:37:08.76	62:14:31.5	2.045	...	GAL	24.94	0.15	0.04	> 25.0	23.68	23.97	...	...	...		
BM1163	12:37:26.98	62:12:24.5	1.876	1.872	GAL	24.72	0.23	0.43	23.80	23.56	23.18	...	22.74	...		
BM1171	12:36:40.34	62:18:53.8	...	2.082	GAL	24.71	0.28	0.36	...	...	23.45	23.69	...	...	...	
BM1172	12:37:02.84	62:16:20.5	1.866	1.862	GAL	24.23	0.13	0.15	23.55	23.49	23.60	23.53	...	...	...	
BM1174	12:36:56.40	62:17:09.8	...	:1.670	GAL	24.97	0.11	0.14	> 25.0	> 24.4	22.70	22.95	23.38	23.38	...	
BM1175	12:37:26.35	62:13:38.5	1.778	1.767	GAL	23.94	0.25	0.30	23.28	23.02	22.53	22.55	...	...	14.6	
BM1180	12:37:27.22	62:13:52.9	...	1.598	GAL	23.55	0.20	0.28	22.21	21.84	22.02	21.95	21.97	...	...	
BM1181	12:37:01.75	62:16:53.0	1.747	1.740	GAL	22.56	0.25	0.35	22.03	22.26	22.47	22.51	22.87	23.31	15.4	
BM1190	12:37:06.87	62:17:02.1	1.020	...	QSO	19.81	0.15	-0.02	19.37	19.06	18.63	18.37	18.10	17.79	866.4	B03-344
BM1193	12:37:19.33	62:15:59.1	...	:1.564	GAL	24.36	0.20	0.17	22.93	23.30	...	...	...	...	...	

TABLE 2 — *Continued*

Name	$\alpha$ (J2000.0)	$\delta$ (J2000.0)	$z_{\text{em}}^{\text{a}}$	$z_{\text{abs}}^{\text{b}}$	Type <sup>c</sup>	$\mathcal{R}^{\text{d}}$ (mag)	$G - \mathcal{R}$ (mag)	$U_{\text{n}} - G^{\text{e}}$ (mag)	$J^{\text{f}}$ (mag)	$K_s^{\text{f}}$ (mag)	$m_{3.6\mu\text{m}}$ (mag)	$m_{4.5\mu\text{m}}$ (mag)	$m_{5.8\mu\text{m}}$ (mag)	$m_{8.0\mu\text{m}}$ (mag)	$f_{24\mu\text{m}}$ ( $\mu\text{Jy}$ )	Notes <sup>g</sup>
BM1195	12:37:35.59	62:14:05.9	...	1.289	GAL	23.97	0.28	0.37	...	...	21.84	21.82	21.99	...	50.4	
BM1196	12:37:18.75	62:16:15.0	1.863	—	GAL	24.62	-0.07	0.00	> 25.0	> 24.4	24.12	24.22	...	...	...	
BM1197	12:37:19.39	62:16:21.0	...	1.566	GAL	23.76	0.20	0.34	22.61	22.38	22.32	22.28	22.77	22.90	18.8	
BM1198	12:37:24.06	62:16:05.8	...	1.780	GAL	23.65	0.24	0.43	23.21	22.73	22.38	22.34	22.41	23.05	39.5	
BM1200	12:37:30.85	62:15:29.6	...	2.078	GAL	23.79	0.26	0.41	23.86	22.45	22.85	22.89	22.99	...	16.7	DRG
BM1201	12:37:21.09	62:16:41.9	1.001	...	GAL	24.24	0.09	0.00	23.12	23.26	23.54	24.00	...	...	...	
BM1204	12:37:18.29	62:17:09.1	...	1.489	GAL	23.64	0.08	0.19	22.79	22.65	22.53	22.60	22.96	...	22.4	
BM1205	12:37:42.45	62:14:19.5	1.711	1.711	GAL	24.44	0.11	-0.05	...	...	22.70	22.54	22.58	22.58	9.4	
BM1207	12:37:16.19	62:17:30.3	1.083	...	GAL	23.95	0.23	0.26	23.19	23.18	22.47	23.63	...	...	171.3	
BM1209	12:37:30.87	62:15:55.1	...	1.775	GAL	23.44	0.29	0.40	> 25.0	22.46	22.28	22.49	22.34	...	15.5	DRG
BM1211	12:37:43.19	62:14:49.6	0.960	...	GAL	24.47	0.21	0.15	...	...	23.53	23.84	...	...	...	
BM1212	12:37:24.28	62:17:20.8	...	1.379	GAL	23.65	0.10	0.26	22.83	23.36	22.77	22.74	...	...	18.4	
BM1226	12:37:11.63	62:19:58.2	1.355	...	GAL	24.32	0.28	0.39	...	...	23.12	23.15	...	...	...	
BM1289	12:37:00.02	62:07:46.2	2.380	...	GAL	24.34	0.45	0.59	...	...	24.13	24.38	...	...	20.2	
BM1293	12:36:58.59	62:08:28.2	2.300	...	GAL	24.91	0.50	0.66	...	...	22.51	23.01	...	...	18.3	
BM1299	12:37:01.33	62:08:44.6	...	1.595	GAL	23.31	0.44	0.51	...	...	20.91	21.04	21.10	21.27	...	
BM1303	12:36:39.51	62:11:40.4	...	1.721	GAL	24.75	0.46	0.45	23.56	22.43	22.23	22.03	22.06	22.35	134.7	
BM1324	12:36:16.00	62:15:58.2	0.322	0.322	GAL	22.80	0.36	0.52	...	...	22.45	22.66	22.50	...	12.7	
BM1326	12:36:53.46	62:11:40.0	...	1.268	GAL	22.31	0.28	0.19	21.46	20.47	20.38	20.29	20.48	20.02	303.2	B03-277
BM1334	12:37:12.15	62:10:29.6	...	1.893	GAL	23.74	0.43	0.58	22.47	21.96	21.97	21.89	22.10	22.36	15.3	
BM1335	12:37:07.82	62:10:57.6	...	1.489	GAL	23.16	0.51	0.55	22.02	21.47	21.15	21.05	21.19	...	...	
BM1339	12:37:09.12	62:11:28.5	...	1.338	GAL	23.17	0.36	0.31	22.40	22.00	21.93	22.01	22.37	22.56	38.0	
BM1345	12:37:17.39	62:10:46.7	0.202	...	GAL	22.54	0.37	0.53	21.57	20.87	21.72	21.96	21.89	22.15	...	
BM1358	12:37:01.24	62:15:20.5	...	1.807	GAL	24.07	0.46	0.64	22.33	21.17	21.11	20.97	20.91	21.22	202.8	
BM1362	12:37:07.09	62:14:56.0	...	1.711	GAL	23.24	0.48	0.64	22.32	21.87	22.10	22.07	22.21	22.74	33.9	
BM1369	12:37:07.79	62:15:25.0	...	1.879	GAL	24.56	0.43	0.61	> 25.0	23.21	23.59	23.83	...	...	167.9	DRG
BM1375	12:36:58.58	62:17:15.3	2.113	2.106	GAL	23.91	0.30	0.31	22.92	22.75	21.88	22.09	22.29	22.23	...	
BM1376	12:37:13.85	62:15:38.3	...	1.278	GAL	23.35	0.46	0.40	22.30	22.12	23.69	...	...	...	...	
BM1384	12:37:23.15	62:15:38.0	2.243	...	AGN	23.98	0.49	0.45	22.79	21.69	21.91	21.63	21.27	20.75	63.8	B03-409
BM1396	12:37:38.38	62:15:09.0	1.743	1.743	GAL	23.66	0.45	0.52	...	...	21.48	21.39	21.54	21.81	69.2	
BM1413	12:37:41.39	62:16:45.9	...	1.391	GAL	22.93	0.42	0.35	...	...	22.39	22.73	22.62	...	...	
BM35	12:37:00.80	62:11:34.0	...	1.875	GAL	23.49	0.43	0.17	22.70	22.68	22.66	22.96	...	...	...	
BM63	12:37:13.75	62:14:09.0	1.912	...	GAL	24.48	0.30	0.21	23.87	> 24.4	23.55	23.56	...	...	...	
BM69	12:37:17.68	62:14:35.9	1.991	1.991	GAL	25.12	0.31	0.27	> 25.0	> 24.4	...	...	...	...	32.7	
BM70	12:37:20.05	62:14:57.1	1.997	1.994	GAL	24.05	0.37	0.15	23.11	23.33	23.24	23.69	...	...	...	
BM72	12:37:22.00	62:15:03.3	...	1.571	GAL	24.72	0.34	0.18	23.27	23.33	22.24	...	...	...	...	
C2	12:35:59.42	62:11:19.9	...	2.991	GAL	25.24	0.80	> 1.46	...	...	23.35	23.39	...	...	...	
C11	12:36:47.88	62:10:31.9	...	2.990	GAL	24.59	0.86	> 2.05	> 25.0	23.46	23.72	23.86	23.25	...	S03-M7; DRG	
C12	12:36:51.54	62:10:41.7	...	2.975	GAL	24.41	1.14	> 1.95	24.2	23.18	22.63	22.54	...	...	23.8	S03-M9
C14	12:36:54.95	62:11:43.8	...	2.973	GAL	25.30	1.07	> 1.13	> 25.0	23.79	23.19	23.16	...	...		
C16	12:36:44.07	62:13:11.0	...	2.929	GAL	23.99	1.14	> 2.37	23.26	22.25	22.04	21.93	21.68	21.47	88.8	S03-M18
C17	12:37:09.73	62:10:16.6	...	3.384	GAL	24.75	1.16	> 1.59	> 25.0	> 24.4	...	...	...	...	...	
C18	12:36:23.89	62:15:48.8	3.230	...	GAL	25.15	0.56	> 1.79	23.96	23.36	23.83	23.92	...	...	...	
C20	12:36:24.29	62:15:51.7	2.981	...	GAL	25.28	0.93	> 1.29	> 25.0	> 24.4	...	...	...	...	...	
C29	12:36:48.86	62:15:02.6	3.115	3.105	GAL	24.72	0.73	> 2.05	> 25.0	23.13	23.25	23.36	23.61	23.25	43.9	S03-oC38; DRG
C30	12:36:51.87	62:15:15.4	3.334	3.321	GAL	24.32	0.79	> 2.39	> 25.0	23.56	23.80	23.81	...	...		S03-C24; DRG
C33	12:36:49.01	62:15:42.5	3.136	3.125	GAL	23.77	0.45	> 3.28	23.68	23.65	23.20	23.28	23.22	...	19.0	S03-D15
C35	12:36:43.09	62:16:36.0	...	3.363	GAL	24.71	0.91	> 1.88	> 25.0	23.53	23.09	23.06	...	...	32.8	S03-M32; DRG
C40	12:37:06.19	62:15:10.1	3.246	3.239	GAL	24.53	0.85	> 2.12	23.95	23.28	23.68	23.69	...	...	...	S03-M27
C41	12:37:21.63	62:13:50.4	3.148	...	GAL	25.14	0.29	> 2.07	> 25.0	23.87	23.08	...	...	...		S03-C18
C42	12:36:51.29	62:18:15.0	3.411	...	GAL	24.46	1.06	> 1.98	...	...	23.56	23.39	...	...	...	
C48	12:36:51.81	62:19:06.0	3.206	...	GAL	24.89	0.99	> 1.62	...	...	23.73	23.87	...	...	...	
C53	12:37:23.38	62:16:23.9	3.103	...	GAL	25.04	0.94	> 1.52	> 25.0	> 24.4	24.07	23.98	...	...	13.8	
C54	12:37:05.98	62:19:04.0	3.217	...	GAL	25.34	0.41	> 1.75	...	...	24.44	24.61	...	...	...	
S03-C5	12:36:23.88	62:09:43.0	...	2.664	GAL	24.65	0.71	0.89	24.10	23.54	23.11	23.40	...	...	29.9	S03-C5

Reddy et al.

TABLE 2 — *Continued*

Name	$\alpha$ (J2000.0)	$\delta$ (J2000.0)	$z_{\text{em}}^{\text{a}}$	$z_{\text{abs}}^{\text{b}}$	Type <sup>c</sup>	$\mathcal{R}^{\text{d}}$ (mag)	$G - \mathcal{R}$ (mag)	$U_n - G^{\text{e}}$ (mag)	$J^{\text{f}}$ (mag)	$K_s^{\text{f}}$ (mag)	$m_{3.6\mu\text{m}}$ (mag)	$m_{4.5\mu\text{m}}$ (mag)	$m_{5.8\mu\text{m}}$ (mag)	$m_{8.0\mu\text{m}}$ (mag)	$f_{24\mu\text{m}}$ ( $\mu\text{Jy}$ )	Notes <sup>g</sup>
S03-C7	12:36:37.64	62:10:47.4	...	2.658	GAL	24.36	0.95	1.23	24.41	23.09	24.25	24.56	...	...	20.3	S03-C7
S03-C8	12:36:26.95	62:11:27.0	2.993	2.983	GAL	24.38	0.85	1.81	23.59	23.96	23.41	23.49	...	...	13.3	S03-C8
S03-C17	12:36:51.17	62:13:48.9	3.163	...	GAL	24.84	0.60	0.92	> 25.0	23.91	23.72	...	...	...	28.4	S03-C17
S03-C26	12:37:03.26	62:16:35.0	...	3.239	GAL	23.95	1.31	2.85	23.58	22.66	20.86	21.30	21.50	21.61	43.2	S03-C26
S03-oC14	12:36:50.36	62:10:55.3	2.928	...	GAL	25.61	0.36	1.21	...	...	...	...	...	...	53.3	S03-oC14
S03-oC26	12:36:34.83	62:12:53.6	3.182	...	GAL	25.63	0.40	1.66	...	...	...	...	...	...	...	S03-oC26
S03-oC29	12:36:45.35	62:13:46.7	3.161	...	GAL	25.49	0.64	1.59	...	...	...	...	...	...	...	S03-oC29
S03-oC34	12:36:33.49	62:14:17.9	3.413	...	QSO	25.32	1.05	1.58	24.21	22.92	22.65	22.42	22.21	21.91	19.3	S03-oC34; B03-176
D8	12:35:59.84	62:12:08.7	3.300	...	GAL	25.10	0.93	2.80	...	...	...	...	...	...	...	
D14	12:36:45.02	62:09:40.6	2.983	2.975	GAL	24.97	0.37	1.92	24.69	23.97	...	...	...	...	...	S03-MD10
D16	12:36:17.49	62:13:10.1	2.930	...	GAL	25.06	-0.01	1.76	...	...	24.42	24.79	...	...	9.7	S03-D11
D19	12:36:41.84	62:11:07.1	3.199	3.187	GAL	24.45	0.68	3.23	24.03	23.33	24.07	23.94	...	...	...	S03-MD22
D20	12:36:49.46	62:10:18.5	3.247	...	GAL	25.26	0.76	2.74	24.45	23.22	24.43	24.71	...	...	13.0	
D23	12:36:19.37	62:15:01.9	3.128	3.123	GAL	23.78	0.62	2.45	23.47	22.96	...	...	...	...	...	S03-C22
D25	12:36:46.94	62:12:26.2	2.970	...	GAL	24.25	0.14	1.94	> 25.0	> 24.4	24.86	25.13	...	...	...	S03-D10
D26	12:36:14.69	62:16:22.9	2.975	...	GAL	25.48	0.29	1.79	...	...	24.07	23.97	...	...	18.5	
D28	12:36:47.79	62:12:55.7	...	2.932	GAL	24.02	0.95	2.55	23.38	22.35	22.36	22.30	22.16	22.06	40.1	S03-M17
D29	12:37:16.91	62:10:02.1	3.451	...	GAL	24.09	0.82	3.37	24.06	23.66	24.04	...	...	...	75.0	S03-C6
D32	12:36:42.39	62:14:49.0	2.962	...	GAL	24.87	0.18	2.38	> 25.0	> 24.4	24.11	24.17	...	...	13.0	S03-D14
D34	12:36:37.14	62:15:48.0	2.975	2.970	GAL	25.46	0.62	2.22	> 25.0	24.21	23.42	23.65	23.62	...	...	S03-C25
D35	12:36:53.62	62:14:10.3	3.196	...	GAL	24.88	1.00	2.76	24.04	23.50	23.72	23.82	...	...	8.9	S03-M22
D38	12:36:39.27	62:17:13.1	2.944	2.936	GAL	24.48	0.71	2.35	23.92	23.32	23.07	23.01	22.72	22.69	...	S03-C27
D39	12:37:00.54	62:14:41.9	...	2.987	GAL	24.82	0.61	2.14	24.60	> 24.4	24.36	...	...	...		
D41	12:36:43.42	62:17:51.8	3.228	...	GAL	24.77	0.84	3.20	24.19	23.46	23.86	23.84	...	23.92	...	
D45	12:36:58.98	62:17:14.2	3.134	3.127	GAL	23.58	1.05	3.09	21.86	20.92	20.93	21.22	21.43	21.44	...	S03-C28
D47	12:37:24.37	62:14:31.9	3.193	3.188	GAL	25.16	0.44	3.23	> 25.0	> 24.4	24.35	24.21	...	...	...	
D55	12:36:55.29	62:19:47.9	3.251	3.239	GAL	23.92	1.14	2.86	...	...	23.27	23.22	23.35	23.04	...	
S03-D3	12:36:47.70	62:10:53.2	...	2.943	GAL	24.18	0.81	1.47	23.68	23.60	...	...	...	...	...	S03-D3
S03-D6	12:37:12.27	62:11:37.8	2.925	...	GAL	25.40	0.14	2.00	...	...	...	...	...	...	35.7	S03-D6
S03-oD3	12:36:48.31	62:09:51.7	2.729	2.720	GAL	24.52	0.68	0.62	> 25.0	24.13	23.86	...	...	...	15.4	S03-oD3
S03-oD12	12:36:20.51	62:14:17.8	2.418	...	GAL	24.59	0.58	0.74	24.18	23.67	23.16	23.10	...	...	96.5	S03-oD12
MD4	12:35:56.54	62:11:26.1	2.867	...	GAL	25.22	0.38	1.55	...	...	23.97	...	...	...	...	
MD6	12:36:02.68	62:10:59.8	3.246	3.241	GAL	24.38	0.87	2.00	...	...	22.70	22.57	...	22.68	114.6	
MD13	12:35:59.63	62:12:00.6	...	2.974	GAL	24.01	0.91	2.31	...	...	22.37	22.57	...	...	...	
MD27	12:36:42.96	62:09:58.1	3.661	...	GAL	25.48	1.00	2.46	22.86	21.04	20.59	20.50	20.33	20.76	21.0	DRG
MD31	12:36:22.58	62:13:06.5	2.981	...	GAL	24.92	0.53	1.69	24.57	23.13	22.03	21.95	21.70	21.83	13.4	S03-C14; B03-133; DRG
MD33	12:36:25.56	62:13:50.5	...	2.932	GAL	24.40	0.68	1.88	23.42	23.38	22.94	23.03	22.94	23.42	...	
MD34	12:36:41.25	62:12:03.1	3.222	3.214	GAL	24.26	0.91	2.39	24.17	22.78	23.79	23.78	23.97	...	97.3	S03-C11; DRG
MD39	12:36:22.94	62:15:26.7	2.583	...	QSO	20.48	-0.23	0.78	20.19	20.07	20.04	19.98	19.45	18.82	487.9	B03-137
MD43	12:36:40.87	62:13:58.5	...	3.087	GAL	24.04	0.66	2.02	23.01	22.42	22.25	22.48	22.55	22.95	38.6	S03-D13
MD48	12:37:06.64	62:14:00.2	...	2.926	GAL	24.89	0.69	1.79	24.01	23.36	22.74	22.62	22.67	22.46	34.5	S03-M21
MD49	12:37:25.45	62:12:00.9	...	2.850	GAL	23.95	0.62	1.75	24.01	22.96	23.13	23.15	23.13	23.05	15.6	
MD50	12:36:51.43	62:16:08.3	3.238	3.234	GAL	24.77	0.99	2.04	> 25.0	> 24.4	24.09	24.04	...	...	...	
MD54	12:37:32.35	62:13:11.2	2.939	...	GAL	25.10	0.54	1.99	...	...	23.15	23.03	...	...	...	
MD55	12:37:16.11	62:15:26.5	...	2.956	GAL	24.86	0.69	2.13	> 25.0	> 24.4	23.54	23.52	...	...	12.8	
MD74	12:37:01.27	62:21:32.6	2.635	...	GAL	24.45	0.45	1.58	...	...	21.99	21.73	21.34	20.78	123.4	
MD75	12:37:37.09	62:17:04.6	...	2.790	GAL	24.03	1.08	2.30	...	...	22.19	22.63	22.70	22.73	25.4	
MD78	12:37:07.72	62:21:00.3	2.812	...	GAL	24.83	0.27	1.51	...	...	...	...	...	...	...	
MD79	12:37:10.91	62:20:44.7	...	2.291	GAL	24.44	0.35	1.58	...	...	22.92	22.82	22.62	23.01	23.2	
MD83	12:37:21.57	62:20:11.0	...	3.213	GAL	24.35	0.62	1.77	...	...	23.95	24.26	...	...	9.7	
S03-MD3	12:36:33.05	62:09:03.3	2.898	...	GAL	23.94	0.87	1.48	...	...	20.65	21.13	21.46	22.00	22.4	S03-MD3
S03-MD12	12:37:19.86	62:09:54.9	2.647	...	AGN	24.36	0.72	0.92	23.41	22.11	21.59	21.20	20.48	19.85	139.7	S03-MD12; B03-398
S03-MD45	12:37:14.18	62:16:28.6	2.345	...	GAL	23.63	0.57	0.82	22.00	21.50	21.07	20.91	20.97	21.23	178.1	S03-MD45
S03-oMD19	12:36:37.00	62:10:43.8	...	3.241	GAL	24.04	0.68	1.48	23.75	22.72	23.31	23.25	23.23	22.90	18.5	S03-oMD19
S03-oMD56	12:36:38.40	62:15:39.5	0.000	0.000	STAR	23.24	0.82	1.45	23.40	23.75	23.73	24.13	23.79	...	...	S03-oMD56

TABLE 2 — *Continued*

Name	$\alpha$ (J2000.0)	$\delta$ (J2000.0)	$z_{\text{em}}^{\text{a}}$	$z_{\text{abs}}^{\text{b}}$	Type <sup>c</sup>	$\mathcal{R}^{\text{d}}$ (mag)	$G - \mathcal{R}$ (mag)	$U_n - G^{\text{e}}$ (mag)	$J^{\text{f}}$ (mag)	$K_s^{\text{f}}$ (mag)	$m_{3.6\mu\text{m}}$ (mag)	$m_{4.5\mu\text{m}}$ (mag)	$m_{5.8\mu\text{m}}$ (mag)	$m_{8.0\mu\text{m}}$ (mag)	$f_{24\mu\text{m}}$ ( $\mu\text{Jy}$ )	Notes <sup>g</sup>
S03-M16	12:37:17.38	62:12:46.8	...	2.939	GAL	24.67	0.52	1.02	23.99	23.78	23.49	23.52	...	...	32.0	S03-M16
S03-M23	12:37:02.68	62:14:25.9	...	3.214	GAL	24.61	1.09	2.43	...	...	20.83	20.88	21.04	21.08	...	S03-M23
S03-M25	12:36:50.80	62:14:44.5	...	3.106	GAL	24.70	0.82	1.69	> 25.0	23.85	24.32	...	...	...	...	S03-M25
S03-M35	12:36:45.18	62:16:52.1	...	3.229	GAL	24.05	1.24	3.12	23.34	22.57	22.76	22.65	22.35	22.47	23.5	S03-M35

\* Note.—A full version of this table, including magnitude and flux errors, is available in the accompanying machine-readable table and will be available in the electronic edition of the *Astrophysical Journal*.

<sup>a</sup> Emission line redshift. An entry with a colon indicates the redshift is uncertain. A blank entry indicates that an emission line redshift could not be measured.

<sup>b</sup> Absorption line redshift. An entry with a colon indicates the redshift is uncertain. A blank entry indicates that an absorption line redshift could not be measured.

<sup>c</sup> Source type, either galaxy (“GAL”), “AGN”, “QSO”, or “STAR”. The distinction between QSO and AGN classification is based on the line widths, as described in Steidel et al. (2002), where an object is classified as a “QSO” if it has any emission line with  $\text{FWHM} > 2000 \text{ km s}^{-1}$ . AGN identified using other means (X-ray or mid-infrared emission) are discussed in § 6.2.

<sup>d</sup>  $\mathcal{R}$  magnitude in AB units.

<sup>e</sup> Upper limits given for galaxies undetected in  $U_n$ .

<sup>f</sup> A blank entry indicates the object did not lie in the region with near-IR imaging.

<sup>g</sup> Galaxies in common with the LBG survey in the HDF-N are indicated by their names (“S03-XXX”) as given in Steidel et al. (2003). Galaxies with X-ray counterparts within  $1.5''$  are indicated by their names (“B03-XXX”) in the spectroscopic followup to the *Chandra* 2 Ms survey by Barger et al. (2003). Galaxies satisfying the distant red galaxy (DRG) criteria of Franx et al. (2003) are indicated by “DRG”.

TABLE 3  
 STELLAR POPULATION PARAMETERS

Name <sup>a</sup>	<i>z</i>	$E(B-V)_\infty$	Age <sub><math>\infty</math></sub> (Myr)	SFR <sub><math>\infty</math></sub> ( $M_\odot$ yr <sup>-1</sup> )	$M_\infty^*$ ( $10^{10} M_\odot$ )	$\tau^b$ (Myr)	$E(B-V)_\tau$	Age <sub><math>\tau</math></sub> (Myr)	SFR <sub><math>\tau</math></sub> ( $M_\odot$ yr <sup>-1</sup> )	$M_\tau^*$ ( $10^{10} M_\odot$ )	Notes <sup>c</sup>
BX1035	2.236	0.24	20	234	0.466	20	0.24	15	185	0.419	
BX1040	2.468	0.09	2100	14	3.030	200	0.03	571	7	2.220	
BX1042	2.607	0.18	509	36	1.820	200	0.15	321	23	1.810	
BX1050	2.322	0.27	15	118	0.179	50	0.26	15	98	0.173	
BX1051	2.098	0.12	404	24	0.963	100	0.02	286	7	1.100	
BX1055	2.491	0.12	255	37	0.956	100	0.04	227	14	1.210	
BX1060	2.081	0.24	806	64	5.150	100	0.01	509	4	5.810	
BX1064	2.086	0.14	509	22	1.100	100	0.02	321	5	1.230	
BX1065	2.701	0.08	1434	35	5.040	100	0.00	360	10	3.570	
BX1071	1.996	0.21	161	43	0.690	10	0.14	55	2	0.600	
BX1074	1.750	0.20	1139	26	2.970	100	0.09	360	7	2.490	
BX1075	2.221	0.25	128	91	1.160	50	0.09	203	8	2.270	
BX1080	2.390	0.25	203	78	1.590	50	0.11	203	9	2.430	
BX1081	1.801	0.24	286	46	1.310	50	0.06	255	2	2.030	
BX1084	2.437	0.12	227	82	1.860	100	0.05	227	29	2.570	
BX1085	2.236	0.30	10	201	0.201	20	0.08	90	3	0.602	
BX1086	2.444	0.28	20	139	0.277	50	0.06	203	4	1.250	
BX1089	2.049	0.17	1609	33	5.360	100	0.06	404	7	4.160	
BX1100	2.079	0.14	255	68	1.720	50	0.10	114	34	1.510	
BX1104	2.441	0.11	286	37	1.050	100	0.05	227	15	1.280	
BX1106	2.917	0.10	905	29	2.670	100	0.01	321	9	2.160	
BX1116	2.048	0.13	571	29	1.650	100	0.00	360	5	1.900	
BX1121	1.878	0.17	806	45	3.640	100	0.02	404	7	3.850	
BX1125	2.222	0.15	203	15	0.304	50	0.01	203	2	0.456	
BX1129	1.973	0.17	203	122	2.480	50	0.10	143	37	3.110	
BX1140	1.487	0.18	806	13	1.070	100	0.01	454	1	1.240	
BX1145	2.325	0.07	806	7	0.562	200	0.02	454	3	0.571	
BX1157	2.081	0.08	3000	22	6.720	500	0.02	1278	10	5.740	
BX1161	1.891	0.24	203	86	1.740	20	0.17	90	11	1.930	
BX1164	2.593	0.15	15	67	0.101	$\infty$	0.15	15	67	0.101	
BX1166	1.334	0.14	1139	6	0.649	100	0.00	404	1	0.544	
BX1169	1.871	0.17	454	33	1.490	100	0.07	286	10	1.680	
BX1170	2.443	0.20	806	49	3.950	100	0.04	404	7	3.710	
BX1172	2.806	0.20	10	127	0.127	50	0.00	161	5	0.571	
BX1174	2.349	0.07	719	18	1.300	5000	0.07	719	18	1.360	
BX1185	2.205	0.26	719	39	2.820	200	0.21	404	22	2.820	
BX1186	2.079	0.22	10	52	0.052	10	0.20	10	26	0.045	
BX1192	1.996	0.18	2600	36	9.450	100	0.10	404	11	5.980	
BX1197	2.593	0.06	1434	23	3.350	500	0.04	719	19	2.990	
BX1201	2.000	0.15	203	33	0.671	20	0.04	102	3	0.797	
BX1204	2.205	0.21	640	36	2.330	50	0.05	255	3	2.250	
BX1208	2.589	0.20	15	104	0.157	100	0.01	255	7	0.786	
BX1222	2.442	0.21	9	102	0.093	10	0.20	8	69	0.090	
BX1228	1.997	0.35	8	375	0.312	20	0.34	8	276	0.284	
BX1229	1.343	0.26	50	50	0.251	10	0.24	20	25	0.162	
BX1233	2.856	0.07	2200	26	5.780	1000	0.00	2100	10	7.240	
BX1238	2.261	0.14	640	25	1.590	200	0.09	404	13	1.640	
BX1240	2.282	0.14	114	44	0.507	10	0.05	50	3	0.460	
BX1244	1.012	0.28	20	50	0.100	20	0.28	15	40	0.090	
BX1245	2.093	0.01	1015	15	1.540	500	0.00	571	13	1.390	
BX1250	1.855	0.15	640	18	1.150	100	0.07	286	7	1.110	
BX1252	2.931	0.07	255	36	0.917	50	0.00	161	9	1.050	
BX1253	1.933	0.13	1139	19	2.190	200	0.05	571	7	2.240	
BX1264	2.942	0.00	2100	10	2.140	5000	0.00	2100	10	2.640	
BX1265	2.434	0.12	255	34	0.873	50	0.01	180	6	1.060	
BX1267	1.996	0.11	1900	22	4.100	5000	0.10	2500	25	8.120	IRAC
BX1269	2.275	0.24	255	127	3.250	50	0.17	143	41	3.440	
BX1274	2.596	0.10	640	32	2.050	$\infty$	0.10	640	32	2.050	
BX1277	2.268	0.09	454	25	1.110	100	0.00	286	7	1.200	
BX1281	2.410	0.13	509	14	0.694	100	0.00	360	2	0.809	
BX1283	2.427	0.10	2600	17	4.340	200	0.00	719	5	3.260	
BX1284	2.273	0.07	1139	14	1.540	100	0.00	321	5	1.150	
BX1287	1.675	0.28	9	305	0.278	10	0.00	90	0	0.921	
BX1288	2.301	0.08	509	21	1.060	100	0.00	286	7	1.110	
BX1289	2.488	0.17	404	46	1.850	50	0.06	203	7	2.000	
BX1290	2.980	0.00	905	11	1.020	$\infty$	0.00	905	11	1.020	
BX1291	2.052	0.31	7	469	0.339	100	0.31	7	448	0.336	
BX1296	1.988	0.23	3250	56	18.300	5000	0.20	3250	43	19.900	
BX1297	2.274	0.24	2750	37	10.200	200	0.06	806	7	7.550	
BX1303	2.305	0.10	1700	11	1.800	100	0.01	360	3	1.190	
BX1305	2.234	0.15	2100	17	3.480	200	0.01	719	4	2.780	
BX1307	2.002	0.20	404	92	3.720	10	0.18	50	12	1.810	
BX1311	2.484	0.10	286	58	1.660	50	0.00	180	11	1.890	
BX1313	2.635	0.20	15	121	0.183	1000	0.20	15	120	0.183	

TABLE 3 — *Continued*

Name <sup>a</sup>	<i>z</i>	$E(B-V)_\infty$	Age <sub><math>\infty</math></sub> (Myr)	SFR <sub><math>\infty</math></sub> ( $M_\odot$ yr <sup>-1</sup> )	$M^*_\infty$ ( $10^{10} M_\odot$ )	$\tau^b$ (Myr)	$E(B-V)_\tau$	Age <sub><math>\tau</math></sub> (Myr)	SFR <sub><math>\tau</math></sub> ( $M_\odot$ yr <sup>-1</sup> )	$M^*_\tau$ ( $10^{10} M_\odot$ )	Notes <sup>c</sup>
BX1315	1.671	0.22	571	46	2.620	100	0.17	255	22	2.560	
BX1316	2.088	0.13	3000	23	6.980	1000	0.10	1434	18	5.670	
BX1317	1.789	0.18	321	46	1.480	20	0.09	102	4	1.410	<i>K<sub>s</sub></i>
BX1324	1.818	0.34	509	65	3.320	10	0.26	90	0	2.710	
BX1326	2.984	0.00	806	13	1.040	$\infty$	0.00	806	13	1.040	
BX1327	2.209	0.07	1139	16	1.870	200	0.01	509	7	1.750	
BX1330	2.363	0.06	571	27	1.520	100	0.01	255	12	1.410	
BX1332	2.214	0.29	15	282	0.427	20	0.09	90	8	1.400	
BX1334	3.371	0.00	1800	9	1.700	500	0.00	1609	9	10.500	
BX1339	1.988	0.09	1139	13	1.450	100	0.01	321	5	1.090	
BX1343	2.268	0.13	1015	31	3.170	100	0.02	360	7	2.650	
BX1348	1.921	0.09	509	9	0.468	100	0.01	255	4	0.426	
BX1349	1.873	0.33	509	87	4.440	$\infty$	0.33	509	87	4.440	
BX1354	2.088	0.03	321	6	0.199	100	0.00	180	4	0.189	
BX1358	2.943	0.04	641	12	0.753	100	0.00	255	6	0.660	
BX1362	1.664	0.14	1609	16	2.580	200	0.10	509	9	2.160	
BX1363	2.297	0.16	719	37	2.630	100	0.00	404	5	2.760	
BX1364	2.183	0.15	719	29	2.110	100	0.06	321	8	1.980	
BX1368	2.443	0.16	454	61	2.790	100	0.07	286	18	3.000	
BX1376	2.430	0.07	255	16	0.416	50	0.00	143	5	0.426	
BX1378	1.971	0.21	203	56	1.130	20	0.14	81	10	1.100	
BX1387	2.324	0.11	640	14	0.929	200	0.07	360	9	0.897	
BX1388	2.032	0.29	3000	43	13.000	500	0.21	1139	24	10.400	
BX1391	1.906	0.22	203	50	1.010	20	0.14	90	6	1.120	
BX1397	2.133	0.15	1015	30	3.080	100	0.04	360	7	2.650	
BX1399	2.033	0.18	1800	15	2.670	200	0.14	509	9	2.050	
BX1401	2.481	0.18	1139	85	9.650	100	0.01	454	9	8.580	
BX1408	2.482	0.28	640	57	3.680	100	0.15	360	11	3.880	
BX1409	2.237	0.29	2000	34	6.740	100	0.14	454	5	4.810	<i>K<sub>s</sub></i>
BX1420	2.133	0.24	255	87	2.210	50	0.12	180	15	2.720	
BX1425	1.864	0.10	905	10	0.903	100	0.00	321	3	0.769	
BX1427	2.548	0.13	719	29	2.070	100	0.01	360	6	2.050	
BX1431	2.001	0.11	321	24	0.770	100	0.02	255	8	0.918	
BX1434	1.994	0.15	454	21	0.956	200	0.13	286	15	0.931	
BX1439	2.188	0.18	2750	34	9.270	200	0.05	719	9	6.590	<i>K<sub>s</sub></i>
BX1443	1.684	0.30	571	135	7.730	$\infty$	0.30	571	135	7.730	
BX1446	2.320	0.12	321	32	1.040	100	0.05	255	11	1.290	
BX1451	2.245	0.21	905	41	3.740	200	0.18	404	25	3.330	
BX1458	1.864	0.28	509	31	1.570	50	0.13	227	3	1.560	
BX1460	3.134	0.00	2000	14	2.870	2000	0.00	1700	12	3.170	
BX1461	2.107	0.15	255	20	0.514	200	0.14	203	15	0.535	
BX1479	2.377	0.10	905	22	1.950	100	0.03	321	7	1.600	
BX1480	2.545	0.21	203	80	1.630	5000	0.21	203	79	1.640	
BX1485	2.548	0.14	1139	105	11.900	$\infty$	0.14	1139	105	11.900	
BX1495	2.247	0.13	1139	13	1.470	100	0.00	404	2	1.210	
BX1501	1.877	0.18	321	50	1.600	100	0.06	321	10	2.350	
BX1504	2.864	0.09	255	29	0.743	50	0.00	161	7	0.827	
BX1514	2.135	0.17	1900	18	3.450	200	0.06	640	6	2.870	<i>K<sub>s</sub></i>
BX1525	1.689	0.29	1609	39	6.310	200	0.24	509	23	5.350	
BX1530	2.421	0.14	360	29	1.030	500	0.14	286	26	1.010	
BX1535	2.299	0.27	15	159	0.241	20	0.09	90	4	0.797	
BX1542	1.018	0.31	15	25	0.038	200	0.31	15	24	0.038	
BX1559	2.408	0.06	719	21	1.480	$\infty$	0.06	719	21	1.480	
BX1567	2.225	0.19	571	73	4.150	50	0.05	227	9	4.030	
BX1568	1.787	0.23	15	145	0.220	10	0.00	102	0	0.997	
BX1572	1.782	0.34	8	199	0.165	$\infty$	0.34	8	199	0.165	
BX1574	1.808	0.26	806	41	3.270	50	0.14	227	6	2.840	
BX1588	2.221	0.25	143	207	2.960	10	0.15	64	5	3.220	
BX1605	1.974	0.01	571	13	0.723	1000	0.00	454	12	0.689	
BX1616	2.205	0.04	2500	5	1.250	500	0.01	905	4	0.967	
BX1617	2.320	0.12	321	13	0.419	$\infty$	0.12	404	13	0.516	
BX1630	2.220	0.07	456	16	0.727	100	0.01	255	7	0.771	
BX1636	2.300	0.28	255	129	3.300	10	0.24	45	20	1.770	
BX1641	1.433	0.22	10	54	0.055	50	0.22	10	48	0.053	
BX1642	2.007	0.14	360	25	0.914	$\infty$	0.14	360	25	0.914	
BX1650	2.097	0.17	203	85	1.730	50	0.07	161	19	2.270	
BX1694	2.007	0.12	360	38	1.370	100	0.05	255	14	1.650	
BX1708	1.987	0.34	1278	78	9.940	10	0.41	30	84	1.600	
BX1817	1.860	0.37	114	109	1.240	50	0.36	72	74	1.180	
BX1820	2.457	0.34	360	191	6.870	$\infty$	0.34	360	191	6.870	
BX1821	2.590	0.20	286	41	1.180	100	0.10	286	10	1.610	
BX1823	1.818	0.40	2750	69	18.900	200	0.26	719	20	14.300	
BX1826	2.929	0.01	2100	12	2.540	200	0.00	509	8	1.810	
BX1827	1.988	0.46	7	392	0.284	$\infty$	0.46	7	392	0.284	
BX1848	2.648	0.07	571	12	0.700	100	0.00	321	3	0.792	

TABLE 3 — *Continued*

Name <sup>a</sup>	<i>z</i>	$E(B-V)_\infty$	Age <sub><math>\infty</math></sub> (Myr)	SFR <sub><math>\infty</math></sub> ( $M_\odot \text{ yr}^{-1}$ )	$M^*_\infty$ ( $10^{10} M_\odot$ )	$\tau^b$ (Myr)	$E(B-V)_\tau$	Age <sub><math>\tau</math></sub> (Myr)	SFR <sub><math>\tau</math></sub> ( $M_\odot \text{ yr}^{-1}$ )	$M^*_\tau$ ( $10^{10} M_\odot$ )	Notes <sup>c</sup>
BX82	1.023	0.20	404	6	0.225	10	0.01	227	0	0.310	
BX84	2.163	0.16	1278	38	4.860	$\infty$	0.16	1278	38	4.860	
BX150	2.277	0.16	2400	26	6.290	100	0.06	321	10	2.350	
BX184	1.998	0.45	7	676	0.489	$\infty$	0.45	7	676	0.489	
BX305	2.482	0.29	719	88	6.300	100	0.17	360	18	6.290	
BX308	2.376	0.21	719	38	2.730	100	0.03	454	3	3.040	
BX313	2.323	0.15	905	32	2.880	$\infty$	0.15	905	32	2.880	
BX341	2.117	0.05	905	25	2.280	$\infty$	0.05	905	25	2.280	
BM1008	1.799	0.24	15	149	0.226	200	0.24	15	142	0.223	
BM1011	1.677	0.23	161	53	0.846	20	0.14	102	4	1.230	
BM1030	1.142	0.35	35	51	0.177	10	0.33	20	22	0.138	
BM1048	1.380	0.17	255	32	0.806	10	0.13	55	2	0.570	
BM1053	1.459	0.04	640	3	0.219	200	0.02	321	2	0.197	
BM1061	2.089	0.00	3000	4	1.070	$\infty$	0.00	3000	4	1.070	
BM1063	2.087	0.10	3000	14	4.150	200	0.01	640	6	2.740	
BM1064	1.524	0.17	255	28	0.708	10	0.04	114	0	0.971	
BM1069	2.028	0.14	3000	29	8.650	500	0.06	1434	9	7.850	
BM1072	1.143	0.27	15	74	0.112	10	0.28	10	61	0.105	
BM1092	1.479	0.26	20	66	0.131	20	0.00	180	0	0.759	
BM1095	1.447	0.07	571	7	0.387	50	0.00	203	1	0.382	
BM1098	1.671	0.22	255	51	1.290	10	0.14	72	1	1.220	
BM1122	1.990	0.16	30	57	0.172	20	0.15	20	43	0.147	
BM1135	1.872	0.20	905	55	4.990	1000	0.20	640	52	4.660	
BM1139	1.919	0.07	1139	18	2.040	$\infty$	0.07	1139	18	2.040	
BM1148	2.049	0.13	20	89	0.178	20	0.12	15	70	0.159	
BM1149	1.630	0.17	15	30	0.045	$\infty$	0.17	15	30	0.045	
BM1153	2.444	0.12	2600	50	13.100	1000	0.04	2600	14	17.800	
BM1155	2.020	0.01	905	11	1.030	2000	0.00	806	10	1.040	
BM1159	1.016	0.12	286	19	0.533	100	0.10	180	11	0.568	
BM1160	1.364	0.23	128	20	0.255	10	0.10	90	0	0.440	
BM1161	2.045	0.00	2750	4	1.190	$\infty$	0.00	2750	4	1.190	
BM1163	1.874	0.20	286	23	0.669	100	0.18	161	16	0.632	
BM1171	2.082	0.07	806	10	0.831	$\infty$	0.07	806	10	0.831	
BM1172	1.864	0.08	321	13	0.423	1000	0.07	286	13	0.416	
BM1175	1.773	0.21	114	53	0.605	$\infty$	0.21	114	53	0.605	
BM1180	1.598	0.18	806	32	2.580	100	0.10	321	10	2.320	
BM1181	1.743	0.30	7	645	0.467	$\infty$	0.30	7	645	0.467	
BM1195	1.289	0.24	640	25	1.610	10	0.28	30	18	0.336	
BM1196	1.863	0.00	404	6	0.238	$\infty$	0.00	404	6	0.238	
BM1197	1.566	0.20	360	30	1.090	10	0.09	114	0	1.280	
BM1198	1.780	0.30	15	203	0.307	10	0.31	10	169	0.290	
BM1200	2.078	0.09	640	23	1.490	1000	0.08	571	20	1.550	
BM1201	1.001	0.04	806	2	0.200	100	0.00	286	1	0.178	
BM1204	1.489	0.12	360	21	0.742	20	0.02	128	1	0.821	
BM1205	1.711	0.04	3500	8	2.720	1000	0.03	1434	7	2.090	
BM1207	1.083	0.31	15	57	0.087	50	0.35	10	88	0.098	
BM1209	1.775	0.34	10	365	0.365	10	0.32	9	222	0.331	
BM1226	1.355	0.35	10	104	0.104	50	0.34	10	90	0.099	
BM1289	2.380	0.23	8	139	0.115	10	0.23	7	108	0.114	
BM1299	1.595	0.35	114	203	2.320	5000	0.35	114	202	2.330	
BM1303	1.721	0.30	719	34	2.470	$\infty$	0.30	719	34	2.470	
BM1334	1.893	0.24	509	58	2.930	100	0.17	255	25	2.900	
BM1335	1.489	0.51	10	1061	1.060	50	0.51	10	914	1.010	
BM1339	1.338	0.37	10	309	0.309	10	0.12	81	0	1.030	
BM1358	1.807	0.34	1278	81	10.400	500	0.32	719	63	10.100	
BM1369	1.879	0.41	7	277	0.200	50	0.44	6	394	0.253	
BM1375	2.109	0.07	2500	23	5.720	500	0.04	905	18	4.520	
BM1396	1.743	0.33	128	143	1.830	20	0.26	81	22	2.400	
BM72	1.571	0.19	1139	14	1.580	200	0.13	454	7	1.190	
C2	2.991	0.20	454	40	1.830	1000	0.34	40	163	0.666	
C11	2.990	0.31	9	326	0.297	20	0.01	114	2	0.895	
C12	2.975	0.39	10	891	0.891	10	0.12	81	1	2.520	
C14	2.973	0.46	8	779	0.648	50	0.46	8	694	0.628	
C16	2.929	0.46	9	2025	1.850	$\infty$	0.46	9	2025	1.850	
C29	3.110	0.11	1015	26	2.690	100	0.00	360	6	2.160	
C30	3.328	0.04	454	25	1.140	200	0.00	321	15	1.160	
C33	3.130	0.03	454	36	1.650	5000	0.02	454	35	1.660	
C35	3.363	0.07	1680	28	4.660	500	0.04	806	20	3.970	
C41	3.148	0.04	2000	15	3.030	1000	0.00	2000	8	5.340	
C42	3.411	0.12	227	55	1.260	2000	0.12	227	53	1.260	
C48	3.206	0.26	15	179	0.270	50	0.02	180	6	1.050	
C53	3.103	0.30	9	249	0.227	200	0.30	9	243	0.227	
S03-C7	2.658	0.34	5	546	0.274	10	0.34	5	397	0.258	
S03-C8	2.988	0.12	255	45	1.140	50	0.00	203	5	1.460	
S03-C17	3.163	0.00	1900	11	2.140	5000	0.00	1900	11	2.470	

TABLE 3 — *Continued*

Name <sup>a</sup>	<i>z</i>	$E(B-V)_\infty$	Age <sub><math>\infty</math></sub> (Myr)	SFR <sub><math>\infty</math></sub> ( $M_\odot \text{ yr}^{-1}$ )	$M^*_\infty$ ( $10^{10} M_\odot$ )	$\tau^b$ (Myr)	$E(B-V)_\tau$	Age <sub><math>\tau</math></sub> (Myr)	SFR <sub><math>\tau</math></sub> ( $M_\odot \text{ yr}^{-1}$ )	$M^*_\tau$ ( $10^{10} M_\odot$ )	Notes <sup>c</sup>
D14	2.979	0.04	2000	13	2.580	1000	0.04	1015	11	1.990	
D16	2.930	0.00	719	8	0.558	$\infty$	0.00	719	8	0.558	
D23	3.125	0.06	1015	47	4.750	200	0.00	454	23	3.910	
D25	2.970	0.07	10	55	0.056	50	0.06	10	49	0.054	
D26	2.975	0.03	2100	7	1.500	2000	0.01	1800	6	1.630	
D28	2.932	0.41	9	1343	1.230	50	0.10	203	16	4.620	
D29	3.451	0.04	203	34	0.697	100	0.01	143	21	0.675	
D32	2.962	0.00	1015	9	0.944	$\infty$	0.00	1015	9	0.944	
D34	2.972	0.14	1139	19	2.190	200	0.04	571	6	2.040	
D35	3.196	0.38	6	787	0.474	10	0.37	6	522	0.432	
D38	2.940	0.23	128	102	1.300	50	0.18	102	44	1.470	
D39	2.987	0.23	10	135	0.135	$\infty$	0.23	10	135	0.135	
D47	3.191	0.00	1278	8	1.050	$\infty$	0.00	1278	8	1.050	
D55	3.245	0.26	9	521	0.475	$\infty$	0.26	9	521	0.475	
S03-oD3	2.725	0.00	806	11	0.906	500	0.00	509	10	0.882	
S03-oD12	2.418	0.28	25	129	0.324	10	0.27	15	74	0.262	
MD4	2.867	0.07	905	12	1.120	500	0.06	571	10	1.060	
MD6	3.243	0.05	1900	34	6.460	200	0.00	571	15	4.910	
MD13	2.974	0.19	321	112	3.600	50	0.04	227	9	4.190	
MD33	2.932	0.34	8	706	0.587	50	0.00	227	5	2.150	
MD48	2.926	0.16	1434	37	5.280	200	0.11	509	19	4.410	
MD49	2.850	0.29	9	485	0.442	50	0.00	203	6	1.780	
MD50	3.236	0.00	905	12	1.090	100	0.00	255	7	0.874	
MD54	2.939	0.12	1900	21	4.070	500	0.10	806	17	3.330	
MD55	2.956	0.20	128	60	0.761	50	0.08	161	10	1.160	
MD75	2.790	0.55	4	7037	2.800	50	0.55	4	6701	2.780	
MD83	3.213	0.00	404	18	0.717	$\infty$	0.00	404	18	0.717	
S03-M16	2.939	0.01	2100	12	2.470	200	0.00	509	8	1.780	
S03-M25	3.106	0.00	1015	11	1.120	200	0.00	360	9	0.904	
S03-M35	3.229	0.35	10	910	0.910	10	0.34	9	558	0.830	

<sup>a</sup> We did not fit the stellar populations of galaxies that had no data longward of  $R$ -band, had uncertain redshifts, or are identified as AGN/QSO from their optical spectra. We also do not present SED parameters for those galaxies with optical and IRAC photometry inconsistent with a simple stellar population (these sources had large  $\chi^2 > 10$  or those sources with  $8 \mu\text{m}$  or  $24 \mu\text{m}$  excesses).

<sup>b</sup> Best-fit star formation history decay timescale in Myr. In some cases, a model with constant star formation ( $\tau = \infty$ ) provided the best-fit.

<sup>c</sup> Objects with large  $K_s$ -band residuals are indicated (i.e., those sources whose  $K_s$ -band measurement lies more than  $3 \sigma$  away from the best-fit stellar population). MD31 is the only directly-detected X-ray source which shows no optical signatures of an AGN, has a relatively faint  $24 \mu\text{m}$  flux, and has photometry that is consistent with a stellar population. The IRAC photometry for BX1267 may suffer from a deblending problem and these (IRAC) data were not used in the SED fit.

TABLE 4  
STELLAR MASSES

Sample	$N_{\text{sed}}^{\text{a}}$	$\log[M_{\text{med}}^*/M_{\odot}]^{\text{b}}$	$\log[M^*/M_{\odot}]^{\text{c}}$
BM	51 (3)	9.87 (10.70)	$9.85 \pm 0.58$ ( $10.58 \pm 0.51$ )
BX	157 (7)	10.20 (10.98)	$10.15 \pm 0.52$ ( $10.94 \pm 0.38$ )
LBG	46 (0)	10.05 (...)	$10.03 \pm 0.44$ (...)
<b>Total</b>	254 (10)	10.10 (10.98)	$10.06 \pm 0.53$ ( $10.83 \pm 0.43$ )

<sup>a</sup> Number of galaxies for which we derived best-fit SED parameters (including stellar mass), regardless of whether the galaxies were imaged at  $K_s$ . The parentheses indicate the number of galaxies with *measured*  $K_s < 21.82$ , or  $K_s(\text{Vega}) < 20$ .

<sup>b</sup> Median stellar mass assuming a constant star formation (CSF) history. Numbers in parentheses give the median stellar mass for those galaxies with  $K_s < 21.82$ , or  $K_s(\text{Vega}) < 20$ .

<sup>c</sup> Mean and dispersion of stellar mass distribution assuming a CSF history. Numbers in parentheses give the mean stellar mass and dispersion for those galaxies with  $K_s < 21.82$ , or  $K_s(\text{Vega}) < 20$ .

TABLE 5  
AGN AT  $z > 1.4$ 

Name	z	X-ray? <sup>a</sup>	Optical? <sup>b</sup>	8 $\mu\text{m}$ ? <sup>c</sup>	24 $\mu\text{m}$ ? <sup>d</sup>	Notes <sup>e</sup>
BX1637	2.487	no	yes (AGN)	yes	yes	ACS point source
BX160	2.460	no	yes (AGN)	yes	yes	$K_s = 21.87$
BM1083	2.414	yes	yes (QSO)	yes	yes	
BM1119	1.717	yes	no	yes	yes	$K_s = 21.74$
BM1156	2.211	no <sup>f</sup>	yes (AGN)	yes	yes	very weak X-ray source
BM1384	2.243	yes	yes (AGN)	yes	no	$K_s = 21.69$
MD31	2.981	yes	no	no	no	ACS point source
MD39	2.583	yes	yes (QSO)	yes	yes	$K_s = 20.07$
MD74	2.635	no	no	yes	yes	
S03-oC34	3.413	yes	yes (QSO)	no	no	
S03-MD12	2.647	yes	yes (AGN)	yes	yes	

<sup>a</sup> Indicates if the source lies within 1''5 of an X-ray counterpart in the 2 Ms data (Alexander et al. 2003).

<sup>b</sup> Indicates if the source shows high ionization optical emission lines indicative of AGN/QSO.

<sup>c</sup> Indicates if the source has a significant 8  $\mu\text{m}$  excess compared with the flux at shorter wavelengths, larger than would be expected from a single stellar population.

<sup>d</sup> Indicates if the source has a 24  $\mu\text{m}$  flux  $f_{24\mu\text{m}} > 100 \mu\text{Jy}$ .

<sup>e</sup>  $K_s$  magnitudes are indicated for AGN with  $K_s < 21.82$ , or  $K_s(\text{Vega}) \lesssim 20$ .

<sup>f</sup> BM1156 is not included in the *Chandra* 2 Ms catalogs, but further refinements to the X-ray data reduction procedure yielded a very weak detection (N. Brandt, private communication).